

1 **Late Holocene glacier and climate fluctuations in the Mackenzie**
2 **and Selwyn Mountain Ranges, Northwest Canada**

3 Adam C. Hawkins¹, Brian Menounos^{1,2}, Brent M. Goehring³, Gerald Osborn⁴, Ben M. Peltó⁵,
4 Christopher M. Darvill⁶, Joerg M. Schaefer⁷

5 ¹Department of Geography, Earth, and Environmental Science, University of Northern British
6 Columbia, Prince George, V2M 5Z9, Canada

7 ²Hakai Institute, Campbell River, V9W 2C7, Canada

8 ³Los Alamos National Laboratory, Los Alamos, 87545, USA

9 ⁴Department of Geoscience, University of Calgary, Calgary, T2N 1N4, Canada

10 ⁵Department of Geography, University of British Columbia, Vancouver, V6T 1Z4, Canada

11 ⁶Department of Geography, University of Manchester, Manchester M13 9PL, England

12 ⁷Department of Earth and Environmental Sciences, Lamont-Doherty Earth Observatory, Columbia
13 University, Palisades, 10964, USA

14 *Correspondence to:* Adam C. Hawkins (ahawkins@unbc.ca)

15

16

17 **Abstract.** Over the last century, northwestern Canada experienced some of the highest rates of
18 tropospheric warming globally, which caused glaciers in the region to rapidly retreat. Our study
19 seeks to extend the record of glacier fluctuations and assess climate drivers prior to the
20 instrumental record in the Mackenzie and Selwyn Mountains of northwestern Canada. We
21 collected 27 ¹⁰Be surface exposure ages across nine cirque and valley glacier moraines to constrain
22 the timing of their emplacement. Cirque and valley glaciers in this region reached their greatest
23 Holocene extents in the latter half of the Little Ice Age (1600-1850 CE). Four erratics, 10-250 m
24 distal from late Holocene moraines, yielded ¹⁰Be exposure ages of 10.9-11.6 ka, demonstrating
25 that by ca. 11 ka, alpine glaciers were no more extensive than during the last several hundred years.
26 Estimated temperature change obtained through reconstruction of equilibrium line altitudes show
27 that since ca. 1850 CE, mean annual temperatures rose 0.2-2.3 °C. We use our glacier chronology
28 and the Open Global Glacier Model (OGGM) to estimate that since 1000 CE, glaciers in this region
29 reached a maximum total volume of 34-38 km³ between 1765-1855 CE and have lost nearly half
30 their ice volume by 2019 CE. OGGM was unable to produce modeled glacier lengths that match
31 the timing or magnitude of the maximum glacier extent indicated by the ¹⁰Be chronology.
32 However, when applied to the entire Mackenzie and Selwyn Mountain region, past-millennium
33 OGGM simulations using the Max Planck Institute Earth System Model (MPI-ESM) and the
34 Community Climate System Model 4 (CCSM4) yield late Holocene glacier volume change
35 temporally consistent with our moraine and remote sensing record, while the Meteorological
36 Research Institute Earth System Model 2 (MRI-ESM2) and the Model for Interdisciplinary
37 Research on Climate (MIROC) fail to produce modeled glacier change consistent with our glacier
38 chronology. Finally, OGGM forced by future climate projections under varying greenhouse gas
39 emissions scenarios predict 85 to over 97% glacier volume loss by the end of the 21st century. The
40 loss of glaciers from this region will have profound impacts to local ecosystems and communities
41 that rely on meltwaters from glacierized catchments.

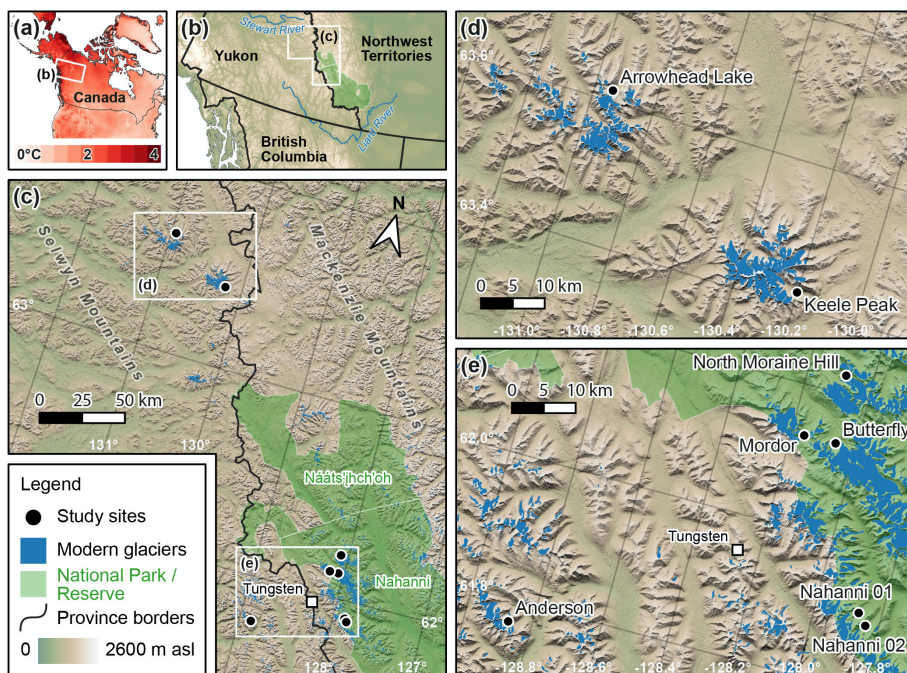
42

43

Deleted:

45 **1 Introduction**

46 Between 1990-2020 CE, northwestern Canada warmed by 1.1 °C above the 1961-1990 CE average
47 (Muñoz-Sabater, 2019, 2021), which contributed to the loss of an estimated $0.429 \pm 0.232 \text{ km}^3$ of
48 ice in the Mackenzie and Selwyn Mountains of eastern Yukon and Northwest Territories between
49 2000 and 2020 CE (Figure 1; Hugonnet et al., 2021). Glaciers in this region are clearly responding
50 to recent climate warming, but proxy evidence of past climate change is scarce (Tomkins et al.,
51 2008; Dyke, 1990). Reconstructions of when and how glaciers responded to past climate change
52 provide one method for estimating paleoclimatic conditions, while also placing the rate of modern
53 glacier change into a geologic context.



54
55 **Figure 1: Study area map of ¹⁰Be sampling locations.** Panel (a) is the temperature trend from ERA5land between 1950 and 2021
56 CE.
57

58 Few glacier change studies exist for the Mackenzie and Selwyn Mountains as compared to other
59 mountainous regions in SW Yukon, British Columbia, and Alaska. Previous Quaternary research
60 in this region focused on Pleistocene glacial deposits and Holocene rock glaciers (i.e. Duk-Rodkin

61 et al., 1996; Fritz et al., 2012; Menounos et al., 2017; Dyke, 1990). The remote location and related
62 logistical challenges of conducting fieldwork in this area are likely reasons this region is
63 underrepresented in Holocene climate reconstructions (e.g. Marcott et al., 2013).

64

65 The timing and magnitude of the most extensive Holocene glacier expansion in the eastern Yukon
66 and Northwest Territories, which places modern glacier retreat in context, remains uncertain.

67 Research in northern and interior Alaska indicates that glaciers reached their maximum Holocene
68 extents around 3.0-2.0 ka (Badding et al., 2013) while nearly all glaciers in southern Alaska and
69 western Canada reached their greatest Holocene positions around 1600-1850 CE, at the
70 culmination of the Little Ice Age (LIA, ~1300-1850 CE) (Menounos et al., 2009; Barclay et al.,
71 2009; Hawkins et al., 2021).

72

73 The primary objectives of our study are to develop a Holocene glacier chronology in the
74 Mackenzie and Selwyn mountains of eastern Yukon and Northwest Territories and use our glacier
75 chronology to estimate changes in climate responsible for these glacier fluctuations. We then
76 deepen our understanding of glacier activity in this area by estimating glacier volume change using
77 multiple models of past climate to force a glacier flowline model. Finally, we briefly evaluate
78 future glacier change in this region in response to various greenhouse gas emissions scenarios.

79 2 Study area

80 The Mackenzie and Selwyn ranges extend over 600 km from north of the Liard River in
81 northwestern British Columbia to the Stewart River and northern extent of the Mackenzie Range
82 in northern Yukon (Fig. 1). This region is covered by 650 km² of ice from nearly 1200 glaciers
83 situated among peaks that rise as high as 2952 m above sea level (Pfeffer et al., 2014). Bedrock
84 consists of faulted and folded Paleozoic sedimentary rocks with Early Cretaceous granitic
85 intrusions (Pfeffer et al., 2014; Cecile and Abbott, 1989). A portion of our study area is situated in
86 the Nahanni (Nááts'ihch'oh) National Park Reserve, which was expanded in 2009 to >30,000 km²
87 (Demuth et al., 2014). Glacier runoff within the Nahanni National Park Reserve flows into the
88 Liard River watershed which later joins the Mackenzie River, eventually draining north to the
89 Beaufort Sea. Two of our nine field sites are located nearly 200 kilometers to the northwest of
90 Nahanni National Park Reserve and are situated on or adjacent to the Keele Peak massif, which is

Deleted: The timing and magnitude of the most extensive Holocene glacier expansion in the eastern Yukon and Northwest Territories, which places modern glacier retreat in context, thus remains uncertain.

Deleted: : i)

Deleted: ii)

Deleted:

Deleted: Meltwaters from glaciers

110 similarly composed of Early Cretaceous granitic rock. Meltwater from our study sites on and near
111 the Keele Peak massif flows into the Stewart River, which flows west to the Yukon River and
112 eventually to the Bearing Sea. The watersheds in our study area are culturally and ecologically
113 important for the numerous First Nations communities who have lived on this land for millennia,
114 including the Dënëndeh, Kaska Dena, and Na-Cho Nyak Dun First Nations, among others.

Deleted: s

115 3 Methods

116 Our glacier chronology originates from digitized glacier margins of aerial photos and satellite
117 imagery, and constraining the age of late Holocene moraines using cosmogenic ^{10}Be surface
118 exposure dating. Cosmogenic surface exposure dating relies on the accumulation of rare isotopes,
119 in this case ^{10}Be , in the bedrock surface during periods of exposure at or near the surface of the
120 Earth (Gosse and Phillips, 2001). We use this chronology to estimate paleoclimate conditions in
121 the late Holocene using several methods. First, we estimate past and present equilibrium line
122 altitudes (ELA) using the maximum elevation of lateral moraines (MELM, LIA maximum only),
123 toe-to-headwall altitude ratio (THAR), and accumulation area ratio (AAR) and infer changes in
124 temperature and precipitation from estimated ELA changes (Braithwaite and Raper, 2009; Meier
125 and Post, 1962; Ohmura and Boettcher, 2018). We then estimate the temperature decrease needed
126 to grow glaciers to their late Holocene positions using a flowline glacier model. Additionally, we
127 perturb monthly temperature and precipitation from several General Circulation Model (GCM)
128 simulations of climate since 1000 CE to produce modeled glacier extents that most closely match
129 the terrestrial and remotely sensed record (Taylor et al., 2012) before evaluating past modelled
130 glacier volume change for all glaciers in the Mackenzie and Selwyn mountains. Finally, we model
131 future glacier change in this region under various Representative Concentration Pathways (RCPs;
132 Moss et al., 2010).

Deleted: The mean annual air temperature and average annual precipitation (1966-1990) in Tungsten, YT (61.95° N, 128.25° W, 1143 m a.s.l.) in the northern extent of Nahanni National Park is -5.1 °C and 643 mm, respectively (Env. and Climate Change Canada 2022). Storms are generally sourced from the North Pacific, though northwesterly air associated with the Arctic Low also plays an important role in the regional climate (Tomkins et al., 2008).

Deleted: To summarize our methods, our

Deleted: ,

Deleted: then

Deleted: dating

Deleted: We

Deleted: Then w

Deleted:

Deleted: 0850

133 3.1 Field site selection

134 We selected sampling locations within the Mackenzie and Selwyn Mountain ranges using satellite
135 imagery, aerial photos, and digital elevation data to identify purported late Holocene moraines.
136 We consulted bedrock geologic maps of the area to locate sites that likely contained quartz-bearing
137 lithologies suitable for ^{10}Be surface exposure dating (hereafter ^{10}Be dating), which was then

175 confirmed in hand-samples in the field (Cecile and Abbott, 1989; Gordey, 1992). Helicopters and
176 floatplanes during late summer in 2014, 2016, and 2017 provided access to the field sites.

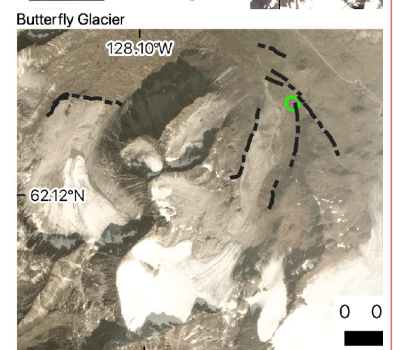
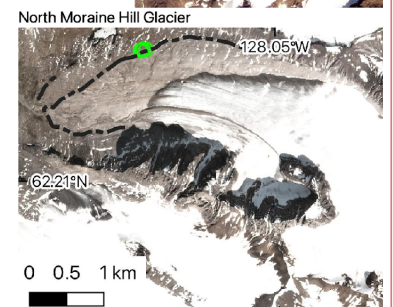
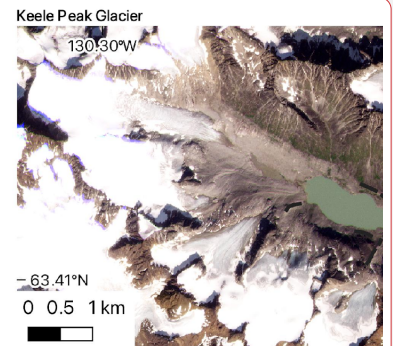
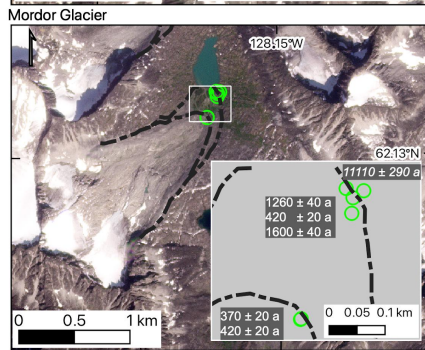
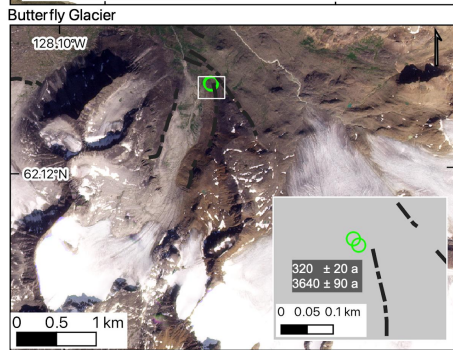
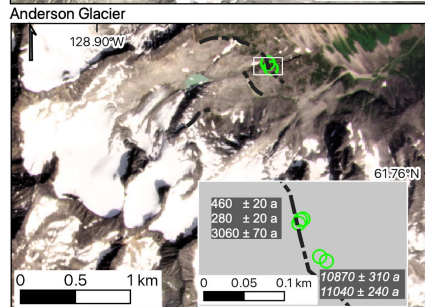
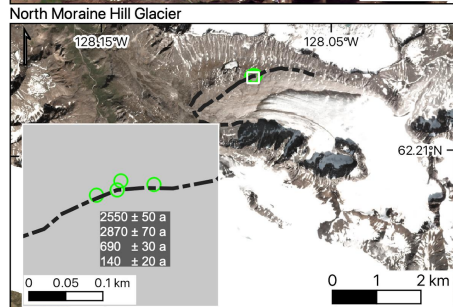
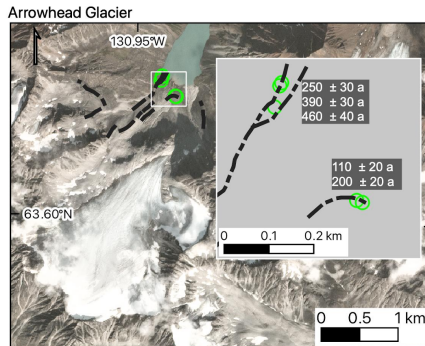
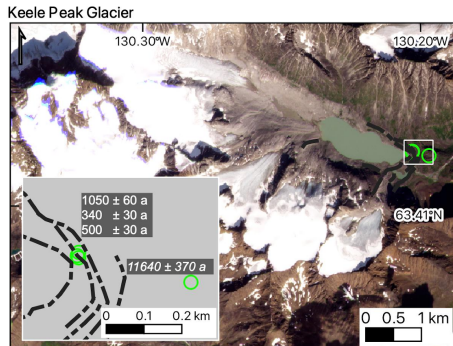
177 3.2 Mapping of former and present glacier extents

178 We manually digitized past glacier outlines for six of the nine glaciers sampled for ¹⁰Be dating.
179 Those glaciers represent sites with multiple dated moraine boulders and morphologies better suited
180 for glacier flowline modeling. ~~It is the author's understanding that only two of the glaciers included~~
181 ~~in this study, North Moraine Hill and Butterfly glaciers, have formal names. The remaining~~
182 ~~glaciers are referred to with informal names below.~~ The resulting glaciers used in paleoclimate
183 reconstructions are Anderson, Mordor, North Moraine Hill, Butterfly, Keele Peak, and Arrowhead
184 glaciers (Fig. 2). We used imagery from airphotos between 1949 and the mid-1970's CE and
185 satellite imagery from 1985 CE, onward (SM Table 2). Air photos represent digitally scanned
186 negatives housed at the Canadian National Airphoto Library (NAPL). We georeferenced each
187 airphoto by manually selecting 40-60 ground control points (GCPs) on the air photographs and
188 high-resolution satellite imagery (e.g. large boulders, peaks, and ridges). We subsequently
189 performed a thin-plate spline transformation in GIS software (QGIS), visually inspecting the
190 georeferenced image for any obvious distortions. Portions of glacier outlines further from GCPs
191 have positional errors smaller than 20 m.

192
193 We used Landsat 5, 7, and 8 satellite imagery to delineate glacier margins at roughly 5-10 year
194 intervals from the mid-1980's onward (SM Figure 12). To aid in the manual digitization, we made
195 false color composites for each Landsat scene to highlight the glacier surface relative to non-
196 glaciated terrain. The surfaces of most glacier termini are debris free, which facilitated glacier
197 mapping. We mapped late Holocene glacier margins using high resolution satellite imagery from
198 Mapbox and PlanetLabs to delineate glacier trimlines and moraine crests. In areas with cloud cover
199 or snow-covered terrain, we used hillshades from ArcticDEM to help identify moraine ridges
200 (Porter et al., 2018).

Deleted: extents

Deleted: Other than North Moraine Hill and Butterfly glaciers, it is the authors' understanding that the remaining glaciers in our study have no formal name.



Deleted:
 Deleted: as
 Deleted:
 Formatted: Font: 9 pt
 Deleted:

213
 214
 215
 216
 217

Figure 2: Glaciers from which ¹⁰Be samples were collected. Sample locations are shown with green circles. Moraine crests are depicted as black dashed lines. Exposure ages ± analytical errors for individual boulders are in text boxes, with erratic boulders ages shown in italics. Grey insets show sampling sites at larger scale. Imagery is from PlanetLabs, acquired between July and August, 2021 and 2022.

231 **3.3 ¹⁰Be field sampling**

232 We targeted samples from large (generally taller than 1 m), granitic boulders on or near moraine
233 crests (Fig. 2, SM [Data](#)). It is commonly assumed that large boulders on moraine crests are
234 windswept such that snow cover is minimal, and their large size limits the chance of being
235 previously covered by moraine material or moving following deposition ([Heyman et al., 2016](#)).
236 Recent work by Tomkins and others (2021) provides evidence that sampling from the crests of
237 moraines may not reduce the chance of geomorphic exposure age scatter, however at the time of
238 sampling in this study, we followed the common practice of targeting boulders on moraine crests.
239 Several erratic boulders directly overlying bedrock and distal to the moraine crests were sampled
240 as well (SM Data). We measured topographic shielding of the incoming cosmic ray flux and
241 boulder self-shielding using a Brunton compass and inclinometer, and then determined the location
242 and elevation of each sample with a handheld GPS receiver with barometric altimeter. Samples
243 were collected from the top surfaces of boulders using a concrete saw and hammer and chisel to
244 collect approximately 1 kg of rock.

Deleted: Fig. 3

245 **3.4 ¹⁰Be laboratory procedures and AMS measurements**

246 The Lamont-Doherty Earth Observatory Cosmogenic Nuclide Laboratory processed samples
247 collected in 2014, and we analyzed the remaining samples in the Tulane University Cosmogenic
248 Nuclide Laboratory. All samples were crushed, milled, and sieved to 250-750 µm. Physical and
249 chemical isolation of quartz was completed following the procedures of Nichols and Goehring
250 (2019). We isolated Be using standard chemical isolation procedures, including anion and cation
251 exchange columns (Ditchburn and Whitehead, 1994; Schaefer et al., 2009). We included a process
252 blank with every batch of ~eight samples (SM Table [3](#)). We sent sample aliquots of extracted Be
253 to either the Purdue Rare Isotope Measurement (PRIME) Laboratory or the Lawrence-Livermore
254 National Laboratory ([LLNL CAMS](#)), for AMS measurements, which were normalized to the
255 standard KNSTD dilution series (Nishiizumi et al., 2007).

Deleted: 1

Deleted:

256
257 We calculated the exposure ages for all samples using version 3 of the online exposure age
258 calculator formerly known as CRONUS-Earth, hosted by the University of Washington
259 (<https://hess.ess.washington.edu/>). We used the default ¹⁰Be reference production rates from the

268 “primary” calibration dataset (Borchers et al., 2016) and report individual sample ages using the
269 Lifton-Sato-Dunai (LSDn) scaling scheme and 1-sigma analytical errors (Table 1). No corrections
270 for burial by snow or surface erosion are applied to the moraines, as snow depth and its variation
271 and rates of surface erosion are poorly constrained. We do, however, provide estimates of how
272 exposure ages may be influenced by snow cover (SM Table 4). Moraine ages are reported as the
273 median exposure age \pm interquartile range to avoid the issue of using statistics that assume an
274 underlying distribution of the ages of the moraine boulders, a key requirement of parametric
275 approaches to characterize central tendency and dispersion (Menounos et al., 2017; Darvill et al.,
276 2022).

- Deleted: ,
- Deleted: these values are
- Deleted: E
- Deleted: taking snow cover into account
- Deleted: with 1 m of 0.25 g
- Deleted:
- Deleted: cm³ snow for 4 months of the year are included in
- Deleted:

Sample	Latitude	Longitude	Elevation (m asl)	Thickness (cm)	Shielding	Quartz (g)	Carrier added (g) ^a	¹⁰ Be/ ⁹ Be ratio	1 sigma uncertainty	Blank-corrected ¹⁰ Be conc. (atoms/g) ^b	Blank-corrected ¹⁰ Be conc. uncertainty (atoms/g)	Exposure age a (LSDs) ^d	Exposure age uncertainty	AMS Facility
Nahanni Nat'l Park area														
<i>Nahanni 01</i>														
14NA-01	61.9075	-127.8688	1500	1.64	0.934	15.01	0.183	6.20E-15	5.32E-16	5.18E+03	4.45E+02	300	30	LLNL-CAMS
14NA-02	61.9075	-127.8686	1500	2.02	0.9272	15.068	0.1836	7.57E-15	5.09E-16	6.36E+03	4.27E+02	370	30	LLNL-CAMS
14NA-03	61.9079	-127.8697	1515	1.9	0.9212	14.023	0.1834	7.79E-14	1.75E-15	6.97E+04	1.53E+03	4060	90	LLNL-CAMS
												Median ± IQR	370 ± 940	
<i>Nahanni 02</i>														
14NA-04	61.8924	-127.8406	1550	1.6	0.9614	15.003	0.1828	1.36E-14	8.85E-16	1.14E+04	7.39E+02	410	40	LLNL-CAMS
14NA-06	61.8925	-127.8404	1550	2.22	0.9595	15.005	0.1827	1.52E-14	1.33E-15	1.27E+04	1.10E+03	670	60	LLNL-CAMS
												Median ± IQR	640 ± 20	
<i>Butterfly Glacier</i>														
14NA-07	62.1299	-128.0637	1710	2.12	0.9837	13.729	0.1833	7.02E-15	4.72E-16	6.46E+03	4.34E+02	320	20	LLNL-CAMS
14NA-09	62.1298	-128.0635	1715	1.93	0.9824	15.032	0.1833	8.88E-14	2.10E-15	7.41E+04	1.78E+03	3640	90	LLNL-CAMS
												Median ± IQR	1980 ± 830	
<i>"Anderson" Glacier</i>														
16-AND-02	61.769	-128.8705	1606	2.5	0.9656	27.207	0.2673	1.41E-14	4.76E-16	8.51E+03	3.46E+02	460	20	LLNL-CAMS
16-AND-03	61.769	-128.8706	1607	2.5	0.9653	28.24	0.2676	9.20E-15	3.88E-16	5.09E+03	2.76E+02	280	20	LLNL-CAMS
16-AND-04	61.769	-128.8706	1608	2.5	0.9656	39.269	0.2681	1.23E-13	2.29E-15	5.56E+04	1.19E+03	3060	70	LLNL-CAMS
16-AND-05	61.7686	-128.87	1605	2.5	0.9628	50.011	0.2672	5.50E-13	1.46E-14	1.96E+05	5.57E+03	10870	310	LLNL-CAMS
16-AND-06	61.7686	-128.8701	1606	2.5	0.9676	50.053	0.2674	5.64E-13	1.05E-14	2.00E+05	4.26E+03	11040	240	LLNL-CAMS
												Median ± IQR	460 ± 700	
<i>"Mordor" Glacier outer moraine</i>														
16-MOR-13	62.1301	-128.1604	1765	2.5	0.9762	37.115	0.2567	6.13E-14	1.54E-15	2.74E+04	8.21E+02	1260	40	LLNL-CAMS
16-MOR-14	62.1302	-128.1606	1764	2.5	0.9765	50.011	0.258	3.06E-14	8.47E-16	8.83E+03	4.96E+02	420	20	LLNL-CAMS
16-MOR-15	62.1298	-128.1604	1765	2.5	0.9792	50.012	0.2583	1.02E-13	1.92E-15	3.45E+04	8.67E+02	1600	40	LLNL-CAMS
16-MOR-16	62.1302	-128.16	1761	2.5	0.9769	50.016	0.2569	6.53E-13	1.53E-14	2.31E+05	5.95E+03	11110	290	LLNL-CAMS
												Median ± IQR	1260 ± 300	
<i>"Mordor" Glacier inner moraine</i>														
16-MOR-11	62.1281	-128.1622	1785	2.5	0.9754	46.672	0.2567	2.51E-14	9.34E-16	7.98E+03	4.02E+02	370	20	LLNL-CAMS
16-MOR-12	62.1281	-128.1622	1762	2.5	0.9754	50.023	0.2572	2.89E-14	8.32E-16	8.81E+03	3.47E+02	420	20	LLNL-CAMS
												Median ± IQR	390 ± 10	
<i>North Moraine Hill Glacier</i>														
16-MH-16	62.2256	-128.0849	1870	2.5	0.9864	50.007	0.2569	1.67E-13	3.12E-15	5.93E+04	1.27E+03	2550	50	LLNL-CAMS
16-MH-17	62.2256	-128.0844	1870	2.5	0.9861	50.002	0.2579	1.91E-13	3.65E-15	6.63E+04	1.52E+03	2870	70	LLNL-CAMS
16-MH-18	62.2257	-128.0835	1869	2.5	0.986	50.005	0.2583	5.28E-14	1.49E-15	1.68E+04	6.81E+02	690	30	LLNL-CAMS
16-MH-19	62.2257	-128.0834	1866	2.5	0.9855	50.022	0.2593	1.42E-14	7.06E-16	2.98E+03	4.57E+02	140	20	LLNL-CAMS
												Median ± IQR	1620 ± 1040	
<i>Keele Peak area</i>														
<i>Keele Peak Glacier</i>														
17-KP-01	63.4201	-130.2021	1548	2.5	0.9726	50.004	0.2587	5.47E-14	2.74E-15	1.94E+04	1.01E+03	1050	60	PRIME
17-KP-02	63.42	-130.2021	1542	2.5	0.9726	49.995	0.2588	1.73E-14	1.27E-15	5.99E+03	4.68E+02	340	30	PRIME
17-KP-03	63.42	-130.2021	1541	2.5	0.9694	48.52	0.259	2.47E-14	1.35E-15	8.91E+03	5.14E+02	500	30	PRIME
17-KP-04	63.4195	-130.1961	1602	2.5	0.9869		0.2587	4.50E-13	9.30E-15	2.16E+05	4.96E+03	11640	270	PRIME
												Median ± IQR	500 ± 180	
<i>Arrowhead Glacier outer moraine</i>														
17-AH-05	63.6162	-130.9434	1410	2.5	0.9364	40.254	0.2593	9.10E-15	9.36E-16	3.76E+03	4.32E+02	250	30	PRIME
17-AH-06	63.6166	-130.9432	1408	2.5	0.9364	44.016	0.2584	1.54E-14	1.18E-15	6.02E+03	4.94E+02	390	30	PRIME
17-AH-07	63.6166	-130.9431	1413	2.5	0.9364	30.637	0.2593	1.27E-14	1.04E-15	7.08E+03	6.27E+02	460	40	PRIME
												Median ± IQR	390 ± 50	
<i>Arrowhead Glacier inner moraine</i>														
17-AH-08	63.6143	-130.9396	1440	2.5	0.9517	50	0.2595	4.90E-15	7.40E-16	1.51E+03	2.79E+02	110	20	PRIME
17-AH-09	63.6143	-130.9393	1440	2.5	0.9517	47.738	0.2594	8.66E-15	8.22E-16	3.01E+03	3.23E+02	200	20	PRIME
												Median ± IQR	150 ± 20	

^a Be Carrier for samples 14-NA* was 1038.3 ug/g, except samples 14-NA(02&07), whose carrier was 1038.8 ug/g. All remaining samples used a PRIME Be carrier with concentration of 1040 ppm.
^b Isotopic ratios were measured at either the Lawrence Livermore National Laboratory - Center for Accelerator Mass Spectrometry (LLNL-CAMS) or the Purdue Rare Isotope Measurement Laboratory (PRIME). Be-10/Be-9 ratios are not corrected for Be-10 detected in procedural blanks.
^c Ages are calculated using version 3 of the online exposure age calculator formerly known as the CRONUS-Earth online exposure age calculator found at <https://hes.us.washington.edu/wrapper> 3.0.2, muons: 1A, constants as of: 2020-08-26). All ages are calculated using the Lifton-Sato-Dunai "LSDn" scaling and the default production rate. Ages and errors are rounded to the nearest decade.
^d The median exposure age and interquartile range (IQR) excludes the exposure age of erratics, whose ages are listed in italics.

Table 1: ¹⁰Be sample information for all boulders sampled in this study.

Deleted: Median and interquartile range calculations exclude erratic boulders sampled outside of moraine boundaries.

3.5 ELA reconstructions

Variations in the equilibrium line altitude of a glacier relate to long term changes in climate. Such variations have been used to estimate changes in either temperature or precipitation (Dahl and Nesje, 1992; Moore et al., 2022; Oien et al., 2022). Commonly used methods to reconstruct past ELAs include the maximum elevation of lateral moraines, toe-to-headwall altitude ratio, and

Deleted: '

312 accumulation area ratio, among others. Each method offers advantages and limitations in
313 reconstructing past ELAs (Benn et al., 2005; Nesje, 1992; Porter, 2001; Osmaston, 2005). We use
314 the MELM, THAR, and AAR methods of ELA reconstruction to estimate glacier ELAs between
315 the Little Ice Age (ca. 1300-1850 CE) and modern time (2000-2021 CE).

Deleted: ELA's

316
317 To record the MELM for each glacier, we used high resolution satellite imagery and elevation data
318 from ASTER GDEM version 3 ([NASA/METI/AIST/Japan Spacesystems and U.S./Japan ASTER](#)
319 [Science Team, 2019](#)) to identify the highest elevation of preserved lateral moraines.

320
321 The THAR method assumes a glacier's ELA is positioned at a fixed ratio between the maximum
322 and minimum elevation of the glacier, shown in Eq. (1):

$$323 \text{ ELA} = \text{minimum glacier elevation} + (\text{glacier elevation range} \times \text{THAR}) \quad (1)$$

324 Work by Meiring (1982) and Murray & Locke (1989) found that ratios of 0.35 to 0.4 yielded
325 satisfactory estimates of alpine glacier ELAs. Here, we use the mean ELA from a THAR of 0.35
326 and 0.4.

Deleted: ELA's

327
328 The accumulation area ratio assumes a fixed ratio of the accumulation area to the total area of a
329 glacier in equilibrium (Braithwaite and Raper, 2009; Meier and Post, 1962). Here, we assume the
330 AAR for glaciers in this region to be 0.6, which is generally considered to be the ratio of steady
331 state cirque and valley glaciers in NW North America (Porter, 1975).

332
333 We generated LIA and modern glacier hypsometries by clipping the ASTER DEM to the digitized
334 glacier extents. In this case, the modern glacier extents are from the latest satellite imagery used
335 for each glacier (imagery from 2017-2021 CE). We acknowledge that the modern DEM does not
336 account for the paleo surface of the glacier during the LIA and may negatively bias the paleo-ELA
337 (Porter, 2001).

Deleted: GDEM version 3, 30 m resolution digital elevation data

Deleted: , between 2017 and 2021 CE.

Deleted: T

338
339 For each ELA reconstruction method, we inferred the change in average temperature (dT) from
340 the Little Ice Age to present as a function of changing ELA by assuming an environmental lapse
341 rate of $-6.5 \text{ }^\circ\text{C km}^{-1}$.

342

362 The ELA of a glacier is also influenced by changes in precipitation. Ohmura et al. (2018; 1992)
363 empirically derive an equation (Eq. 2) to estimate the annual precipitation, P , in millimeters water
364 equivalent (mm w.e.) at the ELA of a glacier, given a mean summer (JJA) temperature T :

$$365 \quad P = a + bT + cT^2, \quad (2)$$

366 where, $a = 966$, $b = 230$, and $c = 5.87$. We estimated changes in precipitation at the ELA of each
367 study glacier by assuming a modern (1986-2015 CE mean) JJA temperature (T) at the modern
368 ELA from the fifth generation European Centre for Medium-Range Weather Forecasts (ECMWF)
369 global climate atmospheric reanalysis (ERA5). We use our dT estimate from our ELA
370 reconstructions to yield Eq. 3:

$$371 \quad P_{LIA} = a + b(T - dT) + c(T - dT)^2 \quad (3)$$

372 We selected ERA5 2 m surface temperatures (Hersbach et al., 2020) from the grid cell nearest to
373 the study glacier and used the same $-6.5 \text{ }^\circ\text{C km}^{-1}$ lapse rate to approximate T at the modern ELA.

374 3.6 Glacier modeling

375 3.6.1 Open Global Glacier Model

376 Our final method of ELA reconstruction uses the Open Global Glacier Model (OGGM; Maussion
377 et al., 2019) which is a modular, open-source model framework with the capacity to model glacier
378 evolution for all glaciers on Earth. The glacier model within OGGM is a depth-integrated flowline
379 model that solves the continuity equation for ice using the shallow ice approximation (Cuffey and
380 Paterson, 2010). Multiple flowlines for each glacier are calculated using a DEM clipped around
381 the glacier polygon using the routing algorithm of Kienholz et al. (2014). The default mass-balance
382 model used in OGGM begins with gridded monthly climate data, here the Climatic Research Unit
383 gridded Time Series (CRU TS) version 4.04 (Harris et al., 2020). The climate data feeds a
384 temperature index model described in Marzeion et al. (2012), incorporating a temperature
385 sensitivity parameter that is calibrated using nearby glaciers with observations of specific mass
386 balance (Zemp et al., 2021). Ice thickness is estimated by assuming a given glacier bed shape
387 (parabolic, rectangular, or mixed) and applying a mass-conservation approach that employs the
388 shallow-ice approximation. OGGM assumes that the “modern” glacier outline, sourced from the
389 Randolph Glacier Inventory (RGI), is from the same date as the DEM. Users are also able to supply

Deleted: d

394 their own glacier outlines. More information on OGGM can be found on OGGM.org, or in
395 publications on the model (Maussion et al., 2019; Eis et al., 2021).

396 3.6.2 Equilibrium run

397 In our first experiment using OGGM, we started with the RGI polygons for the six of our study
398 glaciers targeted for surface exposure dating (Anderson, Mordor, Butterfly, North Moraine Hill,
399 Keele Peak, and Arrowhead glaciers). We then ran a 1000-year simulation under a constant
400 climate, iteratively adjusting a temperature bias relative to the average CRU TS climate centered
401 around 2000 CE (close to the RGI polygon date of most glaciers in the region) until the modeled
402 glacier reached equilibrium at or very near the glacier length indicated by the moraine record.
403 From these equilibrium run experiments, we produce three different estimates of ELA and
404 temperature change. First, the temperature lowering required to expand a glacier to its LIA length
405 was interpreted as the approximate temperature change from the LIA to 2000 CE. Second, we then
406 extracted the hypsometry of the modeled glacier at $t=0$ (modern extent) and $t=1000$ (LIA extent)
407 and estimated the modeled ELA using the same AAR method as described in section 3.5, again
408 assuming an AAR of 0.6. We can again apply the $-6.5\text{ }^{\circ}\text{C km}^{-1}$ lapse rate to estimate the apparent
409 temperature change from modelled glacier extents between the two time periods. Third, for the
410 modern glacier extent, we extracted the elevation at which the modeled surface mass balance of
411 each glacier is equal to zero without any temperature bias. This represents the modern *climatic*
412 ELA and is not based on glacier morphology.

413 3.6.3 Transient run

414 In our next experiment with OGGM, we simulate changes in glacier volume in the Mackenzie and
415 Selwyn mountains using our glacier chronology to tune the climate model input. We used OGGM
416 to simulate the response of our five glaciers driven by monthly temperature and precipitation
417 variability from four Coupled Model Intercomparison Project Phase 5 (CMIP5) GCM runs
418 (CCSM4, MIROC-ESM, MPI-ESM-P, and MRI-ESM2; Taylor et al., 2012). All GCMs
419 incorporate volcanic, total solar irradiance, summer insolation in both hemispheres, aerosol and
420 greenhouse gas emission, and land use change forcings over the period 850-2005 CE (Landrum et
421 al., 2013; Sueyoshi et al., 2013; Yukimoto et al., 2019).

422

423 We omitted the glacier on Keele Peak, as its RGI outline includes several cirque glaciers separated
424 from the main glacier, which causes OGGM to produce a problematic flowline that crosses several
425 flow divides. We set the mass balance gradient for each glacier to 5.2 mm w.e. m⁻¹ based on the
426 mass balance gradient for Bologna Glacier in Nahanni National Park Reserve for the 2014-2015
427 CE balance year (Ednie and Demuth, 2019). For each GCM, we ran 300-500 simulations
428 incrementally perturbing the temperature bias (Tbias) and unitless precipitation factor (Pbias) to
429 determine which combination of temperature and precipitation bias produces a modeled glacier
430 length time series that best fits our glacier chronology. Tbias values ranged from -5 to +2 °C and
431 Pbias between 1.0 and 4.0. Initial testing prior to running the larger simulations showed that Tbias
432 and Pbias values beyond the above range produced glacier extents that far exceeded the late
433 Holocene maximum extent of the glacier or made them disappear entirely. When the glacier
434 flowline exceeded 80 grid points beyond the modern glacier extent, the simulation was discarded.
435 For each simulation, we calculated the summed root mean squared error (RMSE) of modeled
436 glacier length versus the moraine and remotely sensed glacier length at multiple timesteps. The
437 combination of Tbias and Pbias that produced the lowest RMSE was selected as the “optimized”
438 set of parameters for each glacier and GCM. The exact values of Tbias and Pbias are not meant to
439 convey specific information about past climate. These values allow for regional tuning of the
440 OGGM model to better fit the reconstructed and observed glacier response.

441

442 Finally, we averaged the set of Tbias and Pbias from each glacier that produced the lowest RMSE
443 for each GCM and applied those corrections before running simulations of the past millennium for
444 all (1,235) glaciers in the eastern YT/NWT, forced by each “calibrated” GCM. The past
445 millennium climate is of interest as it covers the onset and termination of Little Ice Age cooling.
446 We start all past millennium runs at 1000 CE. We then compared the modeled glacier volume
447 change over the past millennium to our chronology as well as what is already known about late
448 Holocene glacier change in this region to evaluate if the modeling results were reasonable.

449 3.6.4 Future glacier simulations

450 To predict the fate of glaciers in this region, we use OGGM to project 21st-century glacier change
451 for all 1235 glaciers in the eastern Yukon and Northwest Territories, forced by four different

Deleted:

Deleted:

Deleted:

Deleted:

Deleted:

Deleted: Finally

467 CCSM4 projection runs under different representative concentration pathways (RCPs). We use the
468 default model parameters of OGGM v1.5.3 and rely on OGGM's pre-processed glacier directories,
469 which already contain glacier geometry and climate data.

470

471 The historical climate data is CRU TS version 4.04 (Harris et al., 2020). We then download the
472 CMIP5 (CCSM4) climate model output from four different RCP's and run OGGM's bias
473 correction against the CRU calibration data, which in turn calculates anomalies from the CRU
474 reference climatology (1961-1990 CE). Finally, we run OGGM for all 1235 glaciers forced by the
475 calibrated climate scenarios from 2020 to 2100 CE and analyze the projected change in glacier
476 area and volume.

477 **4 Results**

478 **4.1 Glacier chronology**

479 Glaciers in the Mackenzie and Selwyn mountains deposited moraines fronting cirque and valley
480 glaciers 0.7 to 2 km beyond their ca. 2020 CE extents. These moraines are typically devoid of
481 vegetation other than widespread lichen cover. The moraines we sampled are commonly boulder-
482 rich, with pebble-cobble matrices (SM Data).

483

484 Many alpine cirques preserve two nested moraines within tens of meters of each other. We
485 observed nested moraine crests at Keele Peak, Arrowhead, North Moraine Hill, and Mordor
486 glaciers. There is also a partially-nested crest preserved at Anderson Glacier. We did not sample
487 both crests at most locations since our focus was to date the outermost moraines.

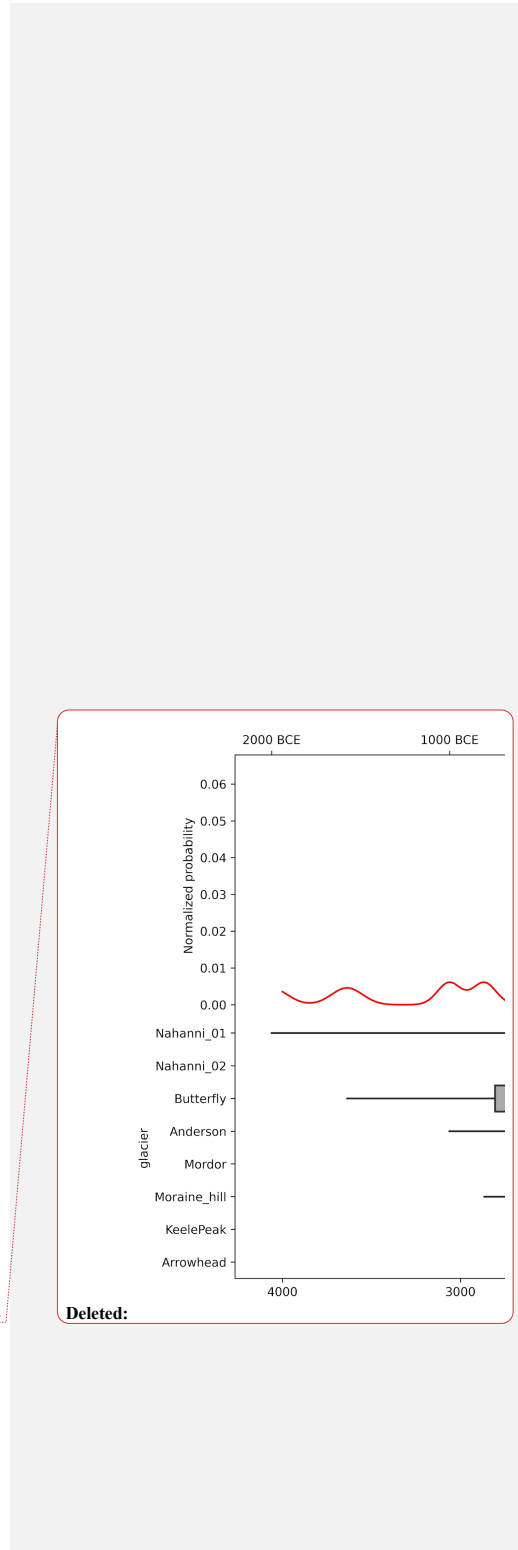
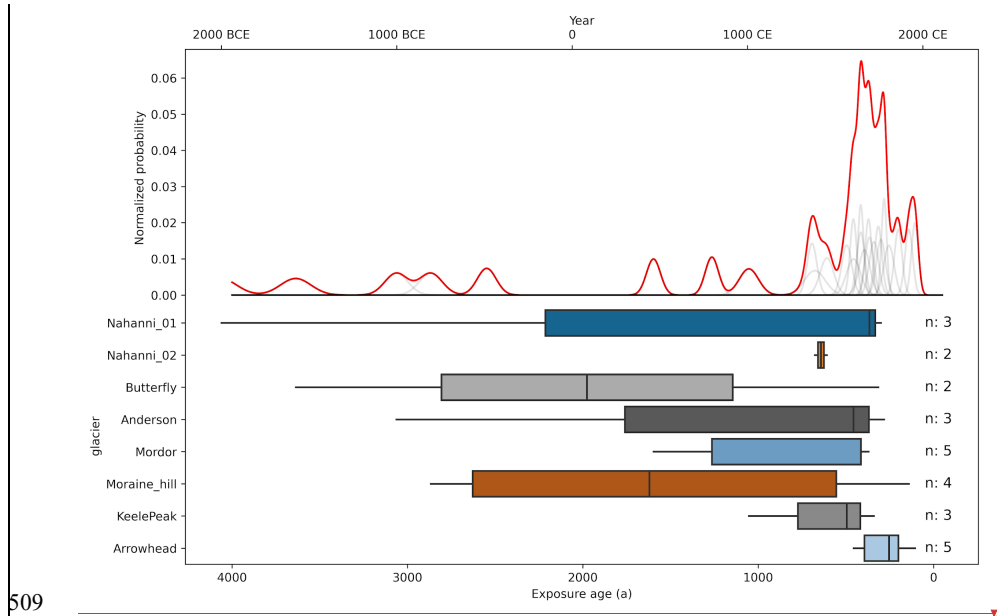
488

489 Erratic boulders 10-40 m beyond cirque moraines at Anderson and Mordor glaciers date to 10.9-
490 11.1 ka (Table 1). An erratic sampled ~250 m beyond the late Holocene moraine fronting Keele
491 Peak glacier dates to 11.6 ± 0.3 ka. Erratic boulders directly overlaid bedrock and had abundant
492 lichen cover. We did not observe any obvious signs of boulder surface erosion, such as
493 grössification, solution pitting, or enhanced relief of resistant minerals.

494

495 In the Nahanni National Park region, the median ^{10}Be age on moraine boulders is 610 ± 850 a (ca.
 496 1405 CE, $n = 19$). Adjacent to Keele Peak, the median moraine exposure age is 370 ± 110 a (ca.
 497 1650 CE, $n = 8$). Together, the sampled moraines in this study date to 460 ± 415 a (ca. 1560 CE).
 498 We sampled both the inner and outer crest of the moraine couplet at Arrowhead and Mordor
 499 glaciers. At Anderson Glacier, the outer moraine dates to 390 ± 50 a (1620 CE, $n = 3$) and the
 500 inner moraine to 150 ± 24 a (1860 CE, $n = 2$). At Mordor Glacier, the outer moraine dates to 1260
 501 ± 295 a (760 CE, $n = 3$) and the inner moraine dates to 390 ± 22 a (1630 CE, $n = 2$).

502
 503 There is notable scatter in the exposure ages on many of the sampled moraines (Table 1, Fig. 3).
 504 At Nahanni 01, Butterfly, Anderson, Mordor, and North Moraine Hill glaciers, there is at least one
 505 sample from each moraine that returned ages older than 1 ka. This scatter gives individual moraine
 506 ages large errors, however when we analyze all moraine boulder ages together, there is a distinct
 507 peak in exposure ages between ~ 800 to 100 a exposure (ca. 1200 to 1900 CE), with the greatest
 508 peak around 480 to 280 a (1540-1740 CE, Fig. 3).



509

512 Figure 3: Box and whisker plots of ^{10}Be surface exposure ages for each glacier, showing the interquartile range and median
 513 age of each moraine surface and the normalized probability density function (red line) for all ^{10}Be samples and kernel
 514 density plot (grey lines) for each individual ^{10}Be sample.

Deleted: .

515 4.2 Climate reconstructions since the late Holocene

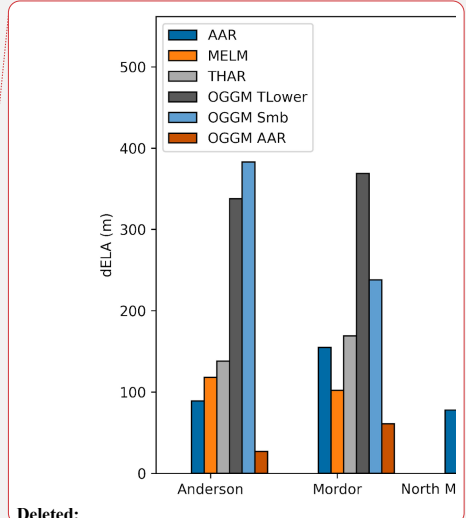
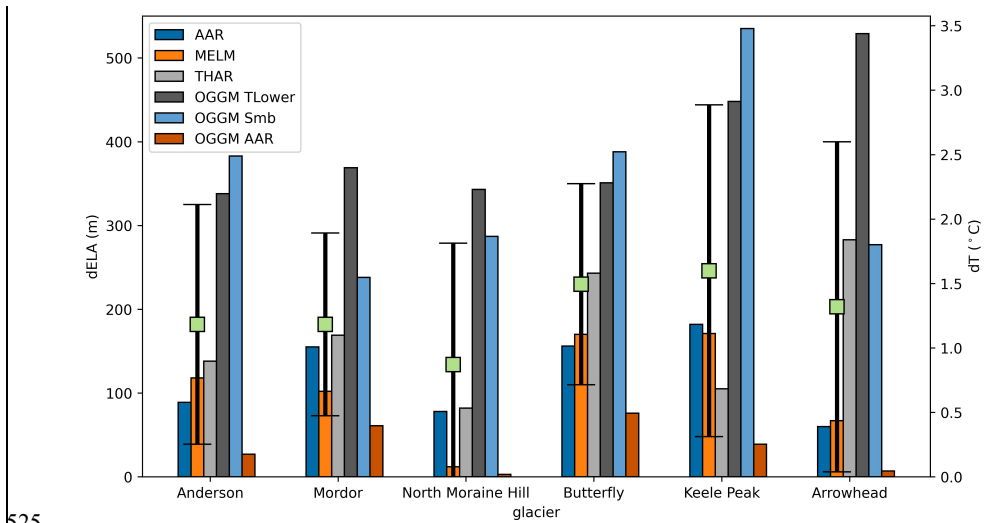
516 ELA reconstruction using the different methods described above yield a range of estimated
 517 changes in ELA between the LIA and modern time (Fig. 4). We use ELAs from the AAR method
 518 using mapped former and modern glacier extents as the “standard” ELA against which we compare
 519 our other ELA estimates. Any ELA reconstruction method could serve as the “standard”; the AAR
 520 method was selected due to its common usage in glacier reconstructions (Benn et al., 2005; Dahl
 521 and Nesje, 1992; Oien et al., 2022). When comparing ELA change within a single method, “dELA”
 522 is the change in reconstructed ELA between the LIA and modern time using the method in
 523 question. As discussed more below, we assume that precipitation remains constant between the
 524 LIA and modern time for ELA reconstructions using the MELM, THAR, and AAR methods.

Deleted: ELA's

Deleted: ,

Deleted: however

Deleted:



Deleted:

526 Figure 4: Changes in ELA and estimated temperature change between the Little Ice Age maximum to modern (ca. 2015)
 527 for six glaciers in this study. Each bar represents a different ELA reconstruction method as described in text. OGGM TLower is
 528 the temperature lowering from ca. 2000 CE climatology required to allow the modeled glacier to reach their late Holocene
 529 maximum extent. OGGM Smb is the change in ELA where the modeled surface mass balance on the glacier equals zero between
 530 the late Holocene maximum and ca. 2000 CE. OGGM AAR is the difference in AAR-derived ELA from the modeled glacier extent
 531 at the late Holocene maximum and ca. 2000 CE. Green squares with capped error bars are the mean and 1-sigma standard deviation
 532 for all ELA reconstruction methods for each glacier.

Deleted:

Deleted: Each method used for reconstruction is discussed in text....

Deleted:

549

550 The modern ELA derived from the AAR method is +12 m to +171 m (average 107 m) higher than
551 the LIA ELA using the maximum elevation of lateral moraines method, corresponding to a +0.1
552 to +1.1 °C (average 0.9 °C) increase in temperature (Fig. 4). Using the THAR method, the dELAs
553 range from +47 m to +240 m (average 138 m), corresponding to a dT of +0.3 to +1.6 °C (average
554 0.9 °C) since the LIA.

555

556 ELAs reconstructed from LIA and modern glacier extent mapping, assuming an AAR of 0.6,
557 indicate a rise in ELA since the LIA of +60 to +182 m, corresponding to a +0.4 to +1.2 °C (average
558 0.8 °C) increase in annual average temperature (Fig. 4).

559

560 Using OGGM, we include three estimates of ELA change. Non-transient simulations on glaciers
561 in the Nahanni National Park region using OGGM require +2.3 °C of warming, relative to the 30-
562 yr average climate centered around 2000 CE, to retreat from their LIA extents to modern positions.
563 Keele Peak and Arrowhead glaciers require nearly +3.2 °C average warming since the LIA relative
564 to their modern temperature (Fig. 4). This warming is equivalent to a dELA since the LIA of +354
565 m in Nahanni National Park and +492 m in the Keele Peak area.

566

567 Applying the AAR method, but with OGGM-derived glacier hypsometries at the LIA and modern
568 time, indicates much less warming since the LIA, with rises in ELAs between +7 m and +76 m,
569 corresponding to a rise in temperature of <0.1 to 0.5 °C. We interpret this minimal change in ELA
570 to be the result of glacier surface thickening in the OGGM model when the glacier expands to LIA
571 extents, which reduces the apparent ELA change as the lower portion of the modeled glacier
572 surface thickens (SM Fig. 5 & 6).

573

574 The third variation of ELA reconstruction using OGGM estimates the modern ELA not from
575 modeled glacier hypsometry, but rather the elevation at which the modeled surface mass balance
576 on the glacier is equal to zero. In a warming climate, this estimate of glacier ELA is expected to
577 be higher than the AAR-derived ELA, as a glacier undergoing rapid retreat has a morphometry
578 that lags behind the climate signal. Changes in ELA using the modern mass balance-derived ELA

Deleted: ELA's

Deleted: ELA's

583 and the AAR-derived LIA ELA range from +277 m to +535 m. Estimated temperature change
584 indicates a rise in temperature since the LIA of +1.6-3.5 °C.

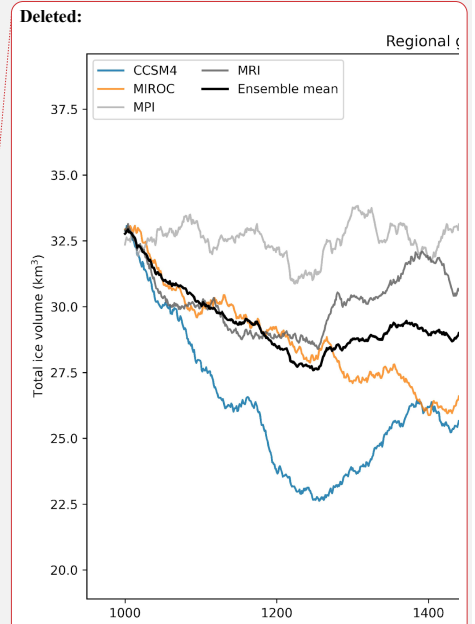
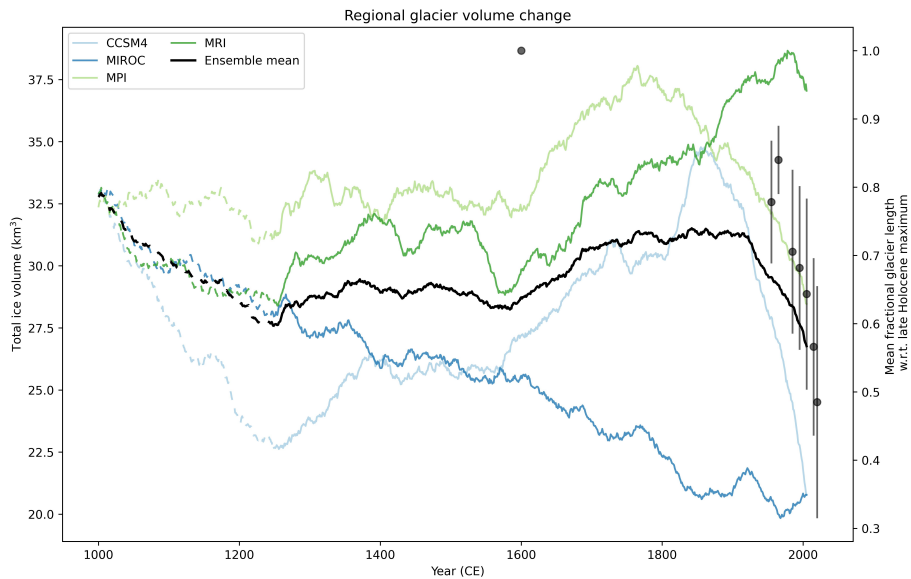
585

586 Using the equation of Ohmura et al. (2018) and temperature change estimates from our AAR-
587 derived ELAs, we estimate that compared to modern values, there was -117 to -339 mm w.e. yr⁻¹,
588 or 5-15% (average 10%), less precipitation at the ELA of our study glaciers during the LIA (SM
589 Table 2).

Deleted: 3

590 4.3 Past millennium glacier change

591 Estimates of glacier evolution in the YT and NWT over the past millennium vary among the four
592 GCMs (Fig. 5). The MPI simulation shows steady glacier volume until 1600 CE, while MRI,
593 MIROC, and CCSM4 indicate a reduction in glacier volume until ca. 1250 CE, afterwards CCSM4
594 and MRI (and to a lesser degree MPI) show an increase in glacier volume until ca. 1400 CE before
595 a period of stable ice volume until ca. 1600 CE. MRI, MPI and CCSM4 all indicate glacier
596 expansion ca. 1600 CE, with MPI reaching a maximum ice volume of 38.1 km³ at 1765 CE and
597 CCSM4 producing a maximum ice volume of 34.7 km³ at 1855 CE (Fig. 5). MRI appears to largely
598 miss 20th century glacier retreat and continues to show glacier expansion until 1980 CE, followed
599 by volume loss. Glacier volume simulated by MIROC decreases through the past millennium, in
600 contrast to the other GCM simulations. Projections of future glacier loss (below) using CCSM4
601 climate simulations begin with an initial regional ice volume of 18.1 km³ in 2019 CE. Compared
602 to the maximum modeled ice volume in the CCSM4 past millennium simulations, this represents
603 a 48% loss in ice volume since ca. 1850 CE.



- Deleted: V
- Deleted:
- Deleted:
- Deleted: with dots
- Deleted: are the
- Deleted: average
- Deleted:
- Deleted: for

606

607 **Figure 5: Modeled ice volume change for all glaciers in the eastern YT and NWT produced by OGGM using four different**
 608 **GCMs. Dashed lines from 1000 CE to 1250 CE are used to indicate spin up duration of the model. Dots and vertical lines**
 609 **respectively denote average and standard deviation (\pm -sigma) of normalized mean glacier length binned by decade.**

610 **4.4 21st Century glacier projections**

611 Under all CCSM4 21st century emissions scenarios, glacier volume in the eastern YT and NWT
 612 significantly declines throughout this century (Fig. 6). Glacier volume is projected to decrease by
 613 85% under RCP2.6 and 97% under RCP8.5, compared to 2019 CE values. The greatest rate of ice
 614 loss is projected to be between present day and ca. 2040 CE, then the rate of volume decline slowly
 615 decreases through to the end of the century.

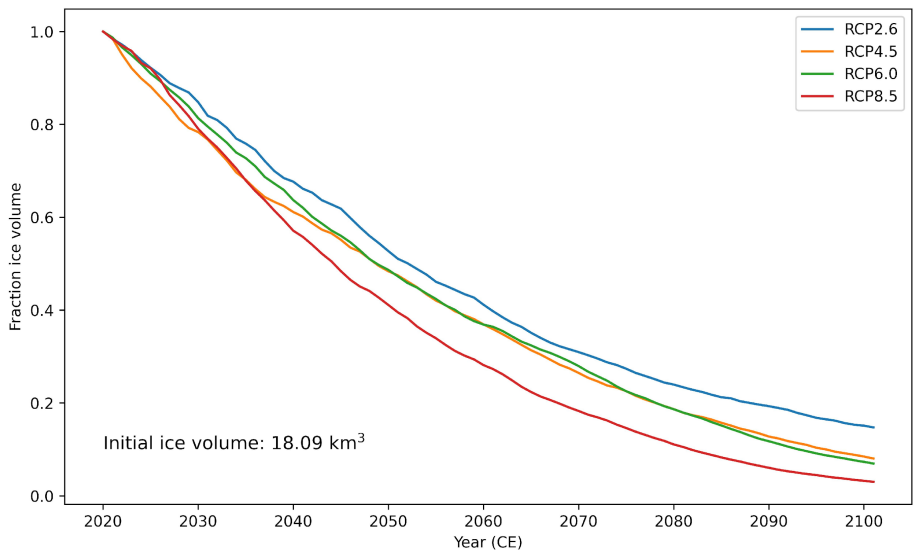


Figure 6: Fractional glacier volume change until 2100 CE under various representative concentration pathways (RCPs) for all glaciers in the eastern YT and NWT.

636
637
638

5 Discussion

639

5.1 Holocene glacier fluctuations

640

641 Early Holocene erratic boulders just beyond moraines dating to the last millennium, as well as a
 642 lack of moraines down valley of the latest Holocene moraines, implies that since ca. 11 ka, glaciers
 643 in this region were no more extensive than during the latest Holocene. These results accord with
 644 records from southern Alaska and western Canada (Menounos et al., 2009; Mood and Smith, 2015;
 645 Barclay et al., 2009) that show most alpine glaciers within these regions reached their greatest
 646 Holocene positions during the last several hundred years. We interpret the erratic boulders of latest
 647 Pleistocene age to record local deglaciation associated with the termination of the Younger Dryas
 648 cold interval (Menounos et al., 2017; Seguinot et al., 2016; Braumann et al., 2022). Similar erratic
 649 boulders that lie beyond late Holocene cirque moraines were dated by Menounos et al. (2017) and
 650 were also interpreted to record local deglaciation. The erratic boulders sampled in the present study
 651 were not part of a moraine, so their ages are interpreted to reflect deglaciation at those sites; the
 652 absence of an associated moraine precludes us from drawing conclusions about the size of the up

Deleted: We

Deleted: feature

664 valley glaciers. The most parsimonious explanation for coeval ages of erratic boulders and end
665 moraines is the complex decay of the Cordilleran Ice Sheet; some cirques were still covered by the
666 ice sheet while others were ice free prior to the Younger Dryas and so were able to form an end
667 moraine (Menounos et al., 2017).

668
669 Our moraine chronology generally accords with the limited previous work in this region. Moraine
670 ages from this study suggest glaciers reached their LIA maximum closer to 1560 CE, with a
671 possible readvance or standstill in the mid-1800's. Tomkins et al. (2008) used varve and tree ring
672 records near Tungsten, YT to infer periods of glacier growth around the late 1300s to 1450 CE,
673 1600 to 1670 CE, 1730 to 1778 CE, and an apparent Little Ice Age maximum 1778-1892 CE. Dyke
674 (1990) completed an extensive lichenometric survey of rock glaciers and late Holocene moraines
675 directly west and south of Tungsten, dating most late Holocene moraines to within the past 400
676 years. Our moraine chronology is in general agreement with the lichenometric ages of Dyke (1990)
677 and suggests an earlier Little Ice Age maximum than interpreted by Tomkins et al. (2008). The
678 significant scatter in our ¹⁰Be moraine dataset complicates our interpretations of decadal-to-
679 century scale glacier fluctuations, however.

680
681 Several scenarios could yield moraine exposure ages that are either older or younger than the
682 true depositional age of the moraine. Inherited nuclides from episodes of previous exposure
683 would result in exposure ages older than the true depositional age. One source of inherited
684 nuclides could be from rockfall followed by supraglacial transport before deposition on the
685 moraine. It is also possible that there was insufficient resetting of the ¹⁰Be inventory in the local
686 bedrock during the Last Glacial Maximum (LGM) as these sites sit at the periphery of the LGM
687 extent of the Cordilleran Ice Sheet. A third possibility is that the inclusion of old outliers reflects
688 the incorporation of previously exposed boulders within the glacier forefield. A review of
689 Holocene glacier fluctuations in western Canada revealed a progressive expansion of ice that
690 culminated with climatic advances during the Little Ice Age (Menounos et al., 2009). Given what
691 is known about Holocene glacier activity, the most likely explanation for our pre Little Ice Age
692 boulder ages is that these boulders contain inherited nuclides from previous moraine building
693 events and were subsequently reincorporated into the late Holocene moraines during the
694 advances of the Little Ice Age.

Deleted: produce
Formatted: Line spacing: 1.5 lines

Deleted: If such with associated ice limits that less
extensivethroughout the HMost glaciers in the Northern
Hemisphere have progressional

Deleted: ¶
¶ We believe the most likely explanation for

Deleted: older late Holocene

711
712 A final possibility to explain the scatter in our moraine ages is that many boulder ages are too
713 young. Mass shielding by previous burial within a moraine followed by exhumation of a sampled
714 boulder, or from snow cover, would reduce the nuclide production rate and result in erroneously
715 young exposure ages. Exhumation and post-depositional movement would be more likely if our
716 moraines were originally ice cored (Crump et al., 2017).

Deleted:

Deleted: Another

Deleted: boulders on our moraines were deposited earlier than their apparent exposure age.

Formatted: Font color: Auto

717
718 Snow cover results in younger apparent ages on moraine boulders, however unrealistic quantities
719 of snow cover are required to meaningfully impact the exposure age of our moraines. One meter
720 of 0.25 g cm⁻³ snow on the surface our boulders for four months of the year would decrease the
721 calculated age by 15-27% (SM Table 4). This decrease in age does not significantly impact our
722 interpretations, as the moraines would still predominately date to the Little Ice Age.

Formatted: Left

723
724 The timing of glacier fluctuations in the eastern Yukon and Northwest Territories agrees with
725 records of late Holocene glacier advance in Europe (Braumann et al., 2020, 2021; Ivy-Ochs et al.,
726 2009). Though Europe has different climate forcings than western North America, the similar
727 timing of late Holocene glacier response suggests that lower temperatures associated with
728 decreasing summer insolation in the Northern Hemisphere played an important role in the timing
729 of glacier advance in the late Holocene in both regions.

Deleted:

730 5.2 ELA and climate reconstruction

731 In this study, we reconstructed and estimated past and present glacier ELAs through several
732 methods, inline with recommendations by Benn et al. (2005) that multiple ELA reconstruction
733 methods be used to provide a more robust estimation of past ELAs and uncertainty with each
734 reconstruction method. An important limitation to the AAR and THAR methods is that they do
735 not account for modern glaciers being out of equilibrium with modern climate. If the modern ELA
736 is not accurately known and the glacier is retreating or advancing in response to climate
737 perturbations, then comparisons in ELA change between modern and other time periods will
738 under- or over-estimate ELA departures (Porter, 2001). Additionally, the assumption that a
739 glacier's ELA only fluctuates due to changes in temperature is an oversimplification (Ohmura et

Deleted: ELA's

Deleted: ELA's

Deleted: it

Deleted: es

756 al., 1992). Increased (decreased) precipitation will lead to a higher (lower) mass balance and may
757 obscure the impact of temperature change on glacier response (i.e. Shea et al., 2004).

758

759 Anderson et al. (2011) presents lacustrine $\delta^{18}\text{O}$ records from the central Yukon that suggest a wet,
760 early Little Ice Age, then dry conditions until modern day, in response to the changing position
761 and strength of the Aleutian Low. If glaciers in the Mackenzie and Selwyn Mountains received
762 greater snowfall during the LIA, then less cooling would be needed to grow glaciers to their LIA
763 extents. Tomkins et al. (2008) developed a July mean temperature reconstruction from tree rings
764 and varved lake sediments close to Tungsten, near the northern end of Nahanni National Park
765 Reserve. Their amalgamated temperature reconstruction demonstrates the differing signals of
766 varved lacustrine sediment and tree ring records but does suggest cooler temperatures in the early
767 1800's, a warm interval at the end of the 1800's to early 1900's, followed by cooling until at least
768 the 1940's before warmer than average July temperatures until modern time.

Deleted: records, but

769

770 Our non-transient experiment using OGGM provides another estimate for temperature change
771 since the LIA, though it still ignores the effect of precipitation variability. By determining the
772 temperature lowering from the present climate needed to grow a modeled glacier to LIA extents,
773 we remove the likely erroneous estimation of the modern glacier ELA based on current glacier
774 hypsometry and more directly compare modern temperatures with the inferred temperature during
775 the LIA maximum, when the glacier was in equilibrium with climate. Both the non-transient
776 ("OGGM TLower" in Fig. 4) and surface mass balance ("OGGM Smb" in Fig. 4) incorporate
777 modern climatology and as a result indicate generally greater temperature change since the LIA
778 compared to glacier geometry-based reconstruction methods. A bedrock borehole temperature
779 reconstruction (62.47° N, 129.22° W) between Nahanni National Park and Keele Peak indicates
780 around +3 °C of surface warming since 1500 CE (Huang et al., 2000), consistent with our
781 temperature change estimates comparing past ELAs to modern climatology. A similar study design
782 as presented in this manuscript would be improved by selecting a site with a multi-year *in situ*
783 mass balance record to compare the modelled modern ELA estimate with the ELA derived from
784 *in situ* measurements.

Deleted: In summary, we recommend that when *in situ* mass balance measurements are not available to determine the modern ELA of a glacier, that modeled ELA's using modern climate be used to estimate present ELA's.

785

793 OGGM is built to perform best at regional to global scales and may produce problematic results at
794 the scale of individual glaciers (Maussion et al., 2019). Differences between the year of DEM
795 acquisition and RGI glacier extent, erroneous glacier margins, and lack of nearby mass balance
796 calibration information can all have significant impacts on the evolution of individual modeled
797 glaciers. To help give confidence that the modeling results from OGGM were producing
798 reasonable glacier evolution, we ran a simple flowline glacier model modified from Jarosch et al.
799 (2013), which was able to grow glaciers to similar extents as OGGM (SM Fig. 2). The similar
800 glacier evolution between the two models indicates that modeled glacier response is the result of
801 climate inputs, rather than unique properties of each model.

802

803 ~~As mentioned above,~~ regular mass balance data from *in situ* mass balance measurements or remote
804 sensing on glaciers in remote areas will help improve the performance **and validation** of global
805 glacier models like OGGM (Eis et al., 2021). A similar study design as is presented in this paper
806 may be successfully implemented in areas with robust glacier chronologies from the late Holocene
807 to present from many more glaciers than are included in our study. Well-constrained glacier
808 chronologies would serve to extend the calibration or validation dataset for large scale glacier
809 modeling efforts (i.e. Rounce et al., 2023).

Deleted: R

810 5.3 GCM evaluation

811 Of the four different CMIP5 GCM simulations tested, glacier model runs forced by CCSM4 and
812 MPI yield glacier fluctuations that best match our general understanding of latest Holocene glacier
813 expansion and glacier retreat over the past millennium (Menounos et al., 2009; Luckman, 2000;
814 Figure 5). We consider the results from MRI to be unreasonable due to the continued ice expansion
815 through most of the 20th century, and similarly discount the results from MIROC due to the
816 modeled steady glacier volume decline over the entire past millennium.

817

818 Our ¹⁰Be chronology suggests glacier advance and moraine formation earlier than what the
819 modeling results show. At Arrowhead Glacier, the outer and inner moraine ¹⁰Be ages (1620 and
820 1860 CE, respectively) are comparable with the modeled glacier evolution under the CCSM4
821 climate, however. MRI suggests a period of glacier retreat shortly before 1600 CE, which is
822 consistent with our moraine chronology, however MRI, CCSM4, and MPI all suggest further ice

827 expansion which would have overridden previously deposited moraines. If the exposure age of a
828 moraine is interpreted to more closely record the onset of glacier retreat, rather than advance, then
829 our moraine chronology further indicates that glaciers reached their LIA maximum extents prior
830 to when OGGM suggests.

831
832 The four GCMs used in our study simulate varied temperature and precipitation time series over
833 the past millennium, which results in differing modeled glacier responses (SM Fig. 8-11). Modeled
834 glaciers forced by CCSM4 and MPI reach late Holocene maxima between 1765 and 1860 CE,
835 coincident with other late Holocene glacier records (Menounos et al., 2009; Barclay et al., 2009;
836 Mood and Smith, 2015). Our moraine and remote sensing record allowed for four GCM's to be
837 calibrated for a small selection of glaciers in the region prior to being run for all 1235 glaciers.
838 Without a well-dated moraine chronology, we would be unable to assess how to model performs
839 beyond the remote sensing record.

840
841 Further research is needed to evaluate why the existing GCM simulations fail to grow glaciers at
842 the same time as our moraine chronology suggests in northwestern Canada. The moraine record
843 offers an important method of validating glacier models beyond the remote sensing record,
844 however moraine chronologies must be tightly constrained in order to confidently evaluate model
845 results. Additional cosmogenic surface exposure dating in this region, especially in areas where
846 there is an unambiguous lack of post-depositional movement may help to produce moraine
847 chronologies with less scatter. Measuring multiple nuclides on moraine boulders (such as using
848 paired $^{14}\text{C}/^{10}\text{Be}$) would allow potential inheritance to be investigated (i.e. Goehring et al., 2022).
849 Finally, as mentioned above, consistent mass balance records from glaciers in this region would
850 help to better constrain the influence of local climate on glacier response in the Mackenzie and
851 Selwyn Mountains (Pelto et al., 2019; Ednie and Demuth, 2019).

852 **5.4 Future response of glaciers to climate change**

853 The Mackenzie and Selwyn mountains are almost certain to experience profound glacier mass loss
854 throughout the 21st century. The estimated magnitude of ice volume decline agrees with modeling
855 results by Clarke et al. (2015) who estimate a 70-95% reduction in glacier volume in the Canadian
856 Rocky Mountains by 2100 CE. Additionally, recent work by Rounce et al. (2023) estimates 93-

857 100% deglaciation in the Mackenzie and Selwyn Mountains by 2100 CE, depending on the
858 magnitude of global temperature change. Under SSP3.7 and SSP5.85, this region is predicted to
859 be fully deglaciated by 2080 CE (Rounce et al., 2023). By 2019 CE, approximately half of the ice
860 volume was lost in the Mackenzie and Selwyn Mountains in the CCSM4 run compared to the
861 glacier maximum in 1860 CE (Fig. 5). The loss of glaciers in this region will cause greater
862 fluctuations in streamflow and temperature that may have negative impacts on thermally stressed
863 species, including fish that are important food sources for local communities (Babaluk et al., 2015;
864 Clason et al., 2023; Moore et al., 2009).↓

Deleted: beyond

865 6 Conclusions

866 Based on geomorphic mapping, surface exposure ages, and numerical modeling, the following
867 conclusions can be drawn from our study. (1) The probability distribution of ¹⁰Be ages suggests
868 that most glaciers in eastern YT and NWT reached their greatest Holocene extents during the
869 latter half of the Little Ice Age [1600-1850 CE]; (2) The uncertainty ascribed to some moraines is
870 high, given the presence of some boulders that yielded ¹⁰Be ages that predate the Little Ice Age,
871 and future work utilizing multi-nuclide approaches would allow this scatter to be further
872 investigated; (3) We find no evidence of glaciers extending beyond LIA limits since at least 10.9-
873 11.6 ka, in accord with most other Holocene glacier records in the Northern Hemisphere; (4) Our
874 ELA reconstructions suggest warming of 0.2-2.3 °C since the LIA, with morphology-based ELA
875 reconstructions likely underestimating the modern ELA of glaciers undergoing retreat; and (5)
876 Projections of future glacier change estimate a further 85-97% loss of glacier volume in the
877 Mackenzie and Selwyn mountains by 2100 CE, in agreement with recent global modeling efforts.

Deleted: t

878
879 Glacier chronologies from late Holocene glacier fluctuations can provide important sources of
880 validation of GCM simulations beyond the instrumental record, especially given the variety
881 between individual GCM simulations of past climate. Nearby *in situ* mass balance records and
882 well-constrained late Holocene glacier chronologies are needed to help validate past millennium
883 GCM simulations and highlight important feedbacks between the arctic and the global climate
884 system. Modern tropospheric warming will continue to dramatically reduce glacier volume in this
885 region, with significant impacts to the local ecosystem that relies on glacier-fed rivers and streams
886 through the summer months.

891
892 *Author Contributions.* Following the CRediT Authorship Guidelines, AH contributed to all 14
893 authorship components except resources and supervision. BM was involved in all authorship
894 components. BG contributed to formal analysis, investigation, resources, supervision, validation,
895 and review/editing. GO was involved in conceptualization, investigation, supervision, and
896 review/editing. BP contributed to data curation, methodology, and software. CD was involved in
897 investigation, visualization, and review/editing. JS was involved in conceptualization, funding
898 acquisition, investigation, and review/editing.

Deleted:Page Break.....

Deleted: Author contributions follow

Deleted: .

899
900 *Competing Interests.*

901 The authors declare that they have no conflict of interest.

902
903 *Acknowledgements.*

904 Funding for this study was provided by a NSERC Northern Supplement and Discovery grant to
905 BM, and a GSA Quaternary Geology and Geomorphology Division Arthur D. Howard Research
906 Award to AH. Additional travel support was provided to AH by the University of Northern British
907 Columbia. The Geological Survey of Canada shared helicopter access in the Nahanni National
908 Park Reserve (NNPR) and graciously allowed us use of their concrete saw. The friendly staff at
909 the Whitehorse Airphoto Library provided invaluable assistance with field site reconnaissance.
910 We are grateful to the Dehcho, Denendeh, and Nahanni Butte First Nations for access to complete
911 our study on their traditional territories. Rebecca Lerch assisted in field work in NNPR. Expert
912 flying by Alpine Aviation provided floatplane access to remote sites around Keele Peak and in
913 NNPR.

914
915 *Code and data availability.*

916 All data described in this paper that have not already been published elsewhere are included within
917 the main text and/or supplementary materials. Code used for glacier modelling has been sourced
918 from OGGM.org or from Jarosch et al. (2013). In the event of paper acceptance and publication,
919 the code will be posted on a publicly available repository under an open-source license.

920
921

931 **References**

- 932 [Anderson, L., Finney, B. P., and Shapley, M. D.: Lake carbonate- \$\delta^{18}\text{O}\$ records from the Yukon](#)
933 [Territory, Canada: Little Ice Age moisture variability and patterns, *Quat. Sci. Rev.*, 30, 887–898,](#)
934 [2011.](#)
- 935 [Babaluk, J. A., Sawatzky, C. D., Watkinson, D. A., Tate, D. P., Mochnacz, N. J., and Reist, J. D.:](#)
936 [Distributions of Fish Species within the South Nahanni River Watershed, Northwest Territories,](#)
937 [91 pp., 2015.](#)
- 938 [Badding, M. E., Briner, J. P., and Kaufman, D. S.: \$^{10}\text{Be}\$ ages of late Pleistocene deglaciation and](#)
939 [Neoglaciation in the north-central Brooks Range, Arctic Alaska, *J. Quat. Sci.*, 28, 95–102, 2013.](#)
- 940 [Barclay, D. J., Wiles, G. C., and Calkin, P. E.: Holocene glacier fluctuations in Alaska, *Quat.*](#)
941 [*Sci. Rev.*, 28, 2034–2048, 2009.](#)
- 942 [Benn, D. I., Owen, L. A., Osmaston, H. A., Seltzer, G. O., Porter, S. C., and Mark, B.:](#)
943 [Reconstruction of equilibrium-line altitudes for tropical and sub-tropical glaciers, *Quat. Int.*,](#)
944 [138–139, 8–21, 2005.](#)
- 945 [Borchers, B., Marrero, S., Balco, G., Caffee, M., Goehring, B., Lifton, N., Nishiizumi, K.,](#)
946 [Phillips, F., Schaefer, J., and Stone, J.: Geological calibration of spallation production rates in the](#)
947 [CRONUS-Earth project, *Quat. Geochronol.*, 31, 188–198, 2016.](#)
- 948 [Braithwaite, R. J. and Raper, S. C. B.: Estimating equilibrium-line altitude \(ELA\) from glacier](#)
949 [inventory data, *Ann. Glaciol.*, 50, 127–132, 2009.](#)
- 950 [Braumann, S. M., Schaefer, J. M., Neuhuber, S. M., Reitner, J. M., Lüthgens, C., and Fiebig, M.:](#)
951 [Holocene glacier change in the Silvretta Massif \(Austrian Alps\) constrained by a new \$^{10}\text{Be}\$](#)
952 [chronology, historical records and modern observations, *Quat. Sci. Rev.*, 245, 106493, 2020.](#)
- 953 [Braumann, S. M., Schaefer, J. M., Neuhuber, S. M., Lüthgens, C., Hidy, A. J., and Fiebig, M.:](#)
954 [Early Holocene cold snaps and their expression in the moraine record of the eastern European](#)
955 [Alps, *Clim. Past*, 17, 2451–2479, 2021.](#)
- 956 [Braumann, S. M., Schaefer, J. M., Neuhuber, S., and Fiebig, M.: Moraines in the Austrian Alps](#)
957 [record repeated phases of glacier stabilization through the Late Glacial and the Early Holocene,](#)
958 [*Sci. Rep.*, 12, 9438, 2022.](#)
- 959 [Cecile, M. P. and Abbott, J. G.: Geology of the Niddery Lake map area \[NTS 105-O\],](#)
960 [https://doi.org/10.4095/130689, 1989.](#)
- 961 [Clarke, G. K. C., Jarosch, A. H., Anslow, F. S., Radić, V., and Menounos, B.: Projected](#)
962 [deglaciation of western Canada in the twenty-first century, *Nat. Geosci.*, 8, 372–377, 2015.](#)
- 963 [Clason, C., Rangecroft, S., Owens, P. N., Lokas, E., Baccolo, G., Selmes, N., Beard, D., Kitch, J.,](#)
964 [Dextre, R. M., Morera, S., and Blake, W.: Contribution of glaciers to water, energy and food](#)
965 [security in mountain regions: current perspectives and future priorities, *Ann. Glaciol.*, 1–6, 2023.](#)

Deleted: Anderson, L., Finney, B. P., and Shapley, M. D.:
Lake carbonate- $\delta^{18}\text{O}$ records from the Yukon Territory,
Canada: Little Ice Age moisture variability and patterns,
Quat. Sci. Rev., 30, 887–898, 2011.¶

... [1]

Formatted: Superscript

997 [Crump, S. E., Anderson, L. S., Miller, G. H., and Anderson, R. S.: Interpreting exposure ages](#)
998 [from ice-cored moraines: a Neoglacial case study on Baffin Island, Arctic Canada, *J. Quat. Sci.*,](#)
999 [32, 1049–1062, 2017.](#)

1000 [Cuffey, K. M. and Paterson, W. S. B.: *The Physics of Glaciers*, Academic Press, 704 pp., 2010.](#)

1001 [Dahl, S. O. and Nesje, A.: Paleoclimatic implications based on equilibrium-line altitude](#)
1002 [depressions of reconstructed Younger Dryas and Holocene cirque glaciers in inner Nordfjord,](#)
1003 [western Norway, *Palaeogeogr. Palaeoclimatol. Palaeoecol.*, 94, 87–97, 1992.](#)

1004 [Darvill, C. M., Menounos, B., Goehring, B. M., and Lesnek, A. J.: Cordilleran ice sheet stability](#)
1005 [during the last deglaciation, *Geophys. Res. Lett.*, 49, <https://doi.org/10.1029/2021gl097191>, 2022.](#)

1006 [Demuth, M. N., Wilson, P., and Haggarty, D.: *Glaciers of the Ragged Range, Nahanni National*](#)
1007 [Park Reserve, Northwest Territories, Canada, in: *Global Land Ice Measurements from Space*,](#)
1008 [edited by: Kargel, J. S., Leonard, G. J., Bishop, M. P., Kääh, A., and Raup, B. H., Springer](#)
1009 [Berlin Heidelberg, Berlin, Heidelberg, 375–383, 2014.](#)

1010 [Ditchburn, R. G. and Whitehead, N. E.: *The separation of ¹⁰Be from silicates*, 1994.](#)

1011 [Duk-Rodkin, A., Barendregt, R. W., Tarnocai, C., and Phillips, F. M.: Late Tertiary to late](#)
1012 [Quaternary record in the Mackenzie Mountains, Northwest Territories, Canada: stratigraphy,](#)
1013 [paleosols, paleomagnetism, and chlorine - 36, *Can. J. Earth Sci.*, 33, 875–895, 1996.](#)

1014 [Dunai, T. J.: *Cosmogenic Nuclides: Principles, Concepts and Applications in the Earth Surface*](#)
1015 [Sciences, Cambridge University Press, 199 pp., 2010.](#)

1016 [Dyke, A. S.: *A lichenometric study of Holocene rock glaciers and neoglacial moraines, Frances*](#)
1017 [Lake map area, southeastern Yukon Territory and Northwest Territories, Geological Survey of](#)
1018 [Canada, 1–33 pp., 1990.](#)

1019 [Ednie, M. and Demuth, M. N.: *Mass balance results from the Cordillera Glacier–Climate*](#)
1020 [Observing Network, British Columbia, Northwest Territories, and Alberta, for 2015 and 2016](#)
1021 [balance years, Geological Survey of Canada, 2019.](#)

1022 [Eis, J., van der Laan, L., Maussion, F., and Marzeion, B.: Reconstruction of past glacier changes](#)
1023 [with an ice-flow glacier model: proof of concept and validation, *Front. Earth Sci.*, 9, 77, 2021.](#)

1024 [Fritz, M., Herzsuh, U., Wetterich, S., Lantuit, H., De Pascale, G. P., Pollard, W. H., and](#)
1025 [Schirrmester, L.: Late glacial and Holocene sedimentation, vegetation, and climate history from](#)
1026 [easternmost Beringia \(northern Yukon Territory, Canada\), *Quat. Res.*, 78, 549–560, 2012.](#)

1027 [Goehring, B. M., Menounos, B., Osborn, G., Hawkins, A., and Ward, B.: Reconciling the](#)
1028 [apparent absence of a Last Glacial Maximum alpine glacial advance, Yukon Territory, Canada,](#)
1029 [through cosmogenic beryllium-10 and carbon-14 measurements, *Geochronology*, 4, 311–322,](#)
1030 [2022.](#)

1031 [Gordey, S. P.: *Geology, Little Nahanni River, Northwest Territories-Yukon Territory*,](#)
1032 [https://doi.org/10.4095/184006, 1992.](#)

Formatted: Justified, Space After: 12 pt

Formatted: Superscript

Deleted:

1061 [Gosse, J. C. and Phillips, F. M.: Terrestrial in situ cosmogenic nuclides: theory and application, Quat. Sci. Rev., 20, 1475–1560, 2001.](#)

1062

1063 [Harris, I., Osborn, T. J., Jones, P., and Lister, D.: Version 4 of the CRU TS monthly high-resolution gridded multivariate climate dataset, <https://doi.org/10.1038/s41597-020-0453-3>, 2020.](#)

1064

1065

1066 [Hawkins, A. C., Menounos, B., Goehring, B. M., Osborn, G. D., Clague, J. J., and Jensen, B.: Tandem dating methods constrain late Holocene glacier advances, southern Coast Mountains, British Columbia, Quat. Sci. Rev., 274, 107282, 2021.](#)

1067

1068

1069 [Hersbach, H., Bell, B., Berrisford, P., Hirahara, S., Horányi, A., Muñoz-Sabater, J., Nicolas, J., Peubey, C., Radu, R., Schepers, D., Simmons, A., Soci, C., Abdalla, S., Abellan, X., Balsamo, G., Bechtold, P., Biavati, G., Bidlot, J., Bonavita, M., Chiara, G., Dahlgren, P., Dee, D., Diamantakis, M., Dragani, R., Flemming, J., Forbes, R., Fuentes, M., Geer, A., Haimberger, L., Healy, S., Hogan, R. J., Hólm, E., Janisková, M., Keeley, S., Laloyaux, P., Lopez, P., Lupu, C., Radnoti, G., Rosnay, P., Rozum, I., Vamborg, F., Villaume, S., and Jean-Noël Thépaut: The ERA5 global reanalysis, Quart. J. Roy. Meteor. Soc., 146, 1999–2049, 2020.](#)

1070

1071

1072

1073

1074

1075

1076 [Heyman, J., Applegate, P. J., Blomdin, R., Gribenski, N., Harbor, J. M., and Stroeven, A. P.: Boulder height – exposure age relationships from a global glacial 10Be compilation, Quat. Geochronol., 34, 1–11, 2016.](#)

1077

1078

1079 [Huang, S., Pollack, H. N., and Shen, P. Y.: Temperature trends over the past five centuries reconstructed from borehole temperatures, Nature, 403, 756–758, 2000.](#)

1080

1081 [Hubbard, A., Willis, I., Sharp, M., Mair, D., Nienow, P., Hubbard, B., and Blatter, H.: Glacier mass-balance determination by remote sensing and high-resolution modelling, J. Glaciol., 46, 491–498, 2000.](#)

1082

1083

1084 [Hugonnet, R., McNabb, R., Berthier, E., Menounos, B., Nuth, C., Girod, L., Farinotti, D., Huss, M., Dussaillant, I., Brun, F., and Käab, A.: Accelerated global glacier mass loss in the early twenty-first century, Nature, 592, 726–731, 2021.](#)

1085

1086

1087 [Ivy-Ochs, S., Kerschner, H., Maisch, M., Christl, M., Kubik, P. W., and Schlüchter, C.: Latest Pleistocene and Holocene glacier variations in the European Alps, Quat. Sci. Rev., 28, 2137–2149, 2009.](#)

1088

1089

1090 [Jackson, L. E., Ward, B., Duk-Rodkin, A., and Hughes, O. L.: The Last Cordilleran Ice Sheet in Southern Yukon Territory, Géographie physique et Quaternaire, 45, 341–354, 1991.](#)

1091

1092 [Jarosch, A. H., Schoof, C. G., and Anslow, F. S.: Restoring mass conservation to shallow ice flow models over complex terrain, <https://doi.org/10.5194/tc-7-229-2013>, 2013.](#)

1093

1094 [Kienholz, C., Rich, J. L., Arendt, A. A., and Hock, R.: A new method for deriving glacier centerlines applied to glaciers in Alaska and northwest Canada, Cryosphere, 8, 503–519, 2014.](#)

1095

1096 [Landrum, L., Otto-Bliesner, B. L., Wahl, E. R., Conley, A., Lawrence, P. J., Rosenbloom, N., and Teng, H.: Last millennium climate and its variability in CCSM4, J. Clim., 26, 1085–1111, 2013.](#)

1097

1098

1125 [Luckman, B. H.: The Little Ice Age in the Canadian Rockies, *Geomorphology*, 32, 357–384,](#)
1126 [2000.](#)

1127 [Marcott, S. A., Shakun, J. D., Clark, P. U., and Mix, A. C.: A reconstruction of regional and](#)
1128 [global temperature for the past 11,300 years, *Science*, 339, 1198–1201, 2013.](#)

1129 [Marzeion, B., Hofer, M., Jarosch, A. H., Kaser, G., and Mölg, T.: A minimal model for](#)
1130 [reconstructing interannual mass balance variability of glaciers in the European Alps, *Cryosphere*,](#)
1131 [6, 71–84, 2012.](#)

1132 [Maussion, F., Butenko, A., Champollion, N., Dusch, M., Eis, J., Fourteau, K., Gregor, P.,](#)
1133 [Jarosch, A. H., Landmann, J., Oesterle, F., Recinos, B., Rothenpieler, T., Vlug, A., Wild, C. T.,](#)
1134 [and Marzeion, B.: The Open Global Glacier Model \(OGGM\) v1.1, *Geosci. Model Dev.*, 12, 909–](#)
1135 [931, 2019.](#)

1136 [Meier, M. F. and Post, A. S.: Recent variations in mass net budgets of glaciers in western North](#)
1137 [America, *International Association of Scientific Hydrology Publications*, 58, 63–77, 1962.](#)

1138 [Meierding, T. C.: Late Pleistocene glacial equilibrium-line altitudes in the Colorado Front](#)
1139 [Range: a comparison of methods, *Quat. Res.*, 18, 289–310, 1982.](#)

1140 [Menounos, B., Osborn, G., Clague, J. J., and Luckman, B. H.: Latest Pleistocene and Holocene](#)
1141 [glacier fluctuations in western Canada, *Quat. Sci. Rev.*, 28, 2049–2074, 2009.](#)

1142 [Menounos, B., Goehring, B. M., Osborn, G., Margold, M., Ward, B., Bond, J., Clarke, G. K. C.,](#)
1143 [Clague, J. J., Lakeman, T., Koch, J., Caffee, M. W., Gosse, J., Stroeven, A. P., Seguinot, J., and](#)
1144 [Heyman, J.: Cordilleran Ice Sheet mass loss preceded climate reversals near the Pleistocene](#)
1145 [Termination, *Science*, 358, 781–784, 2017.](#)

1146 [Mood, B. J. and Smith, D. J.: Holocene glacier activity in the British Columbia Coast Mountains,](#)
1147 [Canada, *Quat. Sci. Rev.*, 128, 14–36, 2015.](#)

1148 [Moore, E. M. M., Eaves, S. R., Norton, K. P., Mackintosh, A. N., Anderson, B. M., Dowling, L.](#)
1149 [H., and Hidy, A. J.: Climate reconstructions for the Last Glacial Maximum from a simple cirque](#)
1150 [glacier in Fiordland, New Zealand, *Quat. Sci. Rev.*, 275, 107281, 2022.](#)

1151 [Moore, R. D., Fleming, S. W., Menounos, B., Wheate, R., Fountain, A., Stahl, K., Holm, K., and](#)
1152 [Jakob, M.: Glacier change in western North America: influences on hydrology, geomorphic](#)
1153 [hazards and water quality, *Hydrol. Process.*, 23, 42–61, 2009.](#)

1154 [Moss, R. H., Edmonds, J. A., Hibbard, K. A., Manning, M. R., Rose, S. K., van Vuuren, D. P.,](#)
1155 [Carter, T. R., Emori, S., Kainuma, M., Kram, T., Meehl, G. A., Mitchell, J. F. B., Nakicenovic,](#)
1156 [N., Riahi, K., Smith, S. J., Stouffer, R. J., Thomson, A. M., Weyant, J. P., and Wilbanks, T. J.:](#)
1157 [The next generation of scenarios for climate change research and assessment, *Nature*, 463, 747–](#)
1158 [756, 2010.](#)

1159 [Muñoz-Sabater, J.: ERA5-Land monthly averaged data from 1981 to present, 2019.](#)

1160 [Muñoz-Sabater, J.: ERA5-Land monthly averaged data from 1950 to 1980, 2021.](#)

Formatted: Justified, Space After: 12 pt

1187 [Murray, D. R. and Locke, W. W.: Dynamics of the late Pleistocene Big Timber Glacier, Crazy](#)
1188 [Mountains, Montana, USA, Journal of Glaciology, 35, 183–190, 1989.](#)

1189 [NASA/METI/AIST/Japan Spacesystems and U.S./Japan ASTER Science Team: ASTER Global](#)
1190 [Digital Elevation Model V003, <https://doi.org/10.5067/ASTER/ASTGTM.003>, 2019.](#)

1191 [Nesje, A.: Topographical effects on the equilibrium-line altitude on glaciers, GeoJournal, 27,](#)
1192 <https://doi.org/10.1007/bf00185102>, 1992.

1193 [Nichols, K. A. and Goehring, B. M.: Isolation of quartz for cosmogenic in situ ¹⁴C analysis,](#)
1194 [Geochronology, 1, 43–52, 2019.](#)

1195 [Nishiizumi, K., Imamura, M., Caffee, M. W., Southon, J. R., Finkel, R. C., and McAninch, J.:](#)
1196 [Absolute calibration of ¹⁰Be AMS standards, Nucl. Instrum. Methods Phys. Res. B, 258, 403–](#)
1197 [413, 2007.](#)

1198 [Ohmura, A. and Boettcher, M.: Climate on the equilibrium line altitudes of glaciers: theoretical](#)
1199 [background behind Ahlmann’s P/T diagram, J. Glaciol., 64, 489–505, 2018.](#)

1200 [Ohmura, A., Kasser, P., and Funk, M.: Climate at the equilibrium line of glaciers, J. Glaciol., 38,](#)
1201 [397–411, 1992.](#)

1202 [Oien, R. P., Rea, B. R., Spagnolo, M., Barr, I. D., and Bingham, R. G.: Testing the area–altitude](#)
1203 [balance ratio \(AABR\) and accumulation–area ratio \(AAR\) methods of calculating glacier](#)
1204 [equilibrium-line altitudes, J. Glaciol., 68, 357–368, 2022.](#)

1205 [Osmaston, H.: Estimates of glacier equilibrium line altitudes by the Area×Altitude, the](#)
1206 [Area×Altitude Balance Ratio and the Area×Altitude Balance Index methods and their validation,](#)
1207 [Quat. Int., 138–139, 22–31, 2005.](#)

1208 [Pelto, B. M., Menounos, B., and Marshall, S. J.: Multi-year evaluation of airborne geodetic](#)
1209 [surveys to estimate seasonal mass balance, Columbia and Rocky Mountains, Canada, Cryosph.](#)
1210 [Discuss., 1–30, 2019.](#)

1211 [Pfeffer, W. T., Tad Pfeffer, W., Arendt, A. A., Bliss, A., Bolch, T., Graham Cogley, J., Gardner,](#)
1212 [A. S., Hagen, J.-O., Hock, R., Kaser, G., Kienholz, C., Miles, E. S., Moholdt, G., Mölg, N., Paul,](#)
1213 [F., Radić, V., Rastner, P., Raup, B. H., Rich, J., Sharp, M. J., and The Randolph Consortium:](#)
1214 [The Randolph Glacier Inventory: a globally complete inventory of glaciers,](#)
1215 <https://doi.org/10.3189/2014jog13j176>, 2014.

1216 [Porter, C., Morin, P., Howat, I., Noh, M.-J., Bates, B., Peterman, K., Keesey, S., Schlenk, M.,](#)
1217 [Gardiner, J., Tomko, K., Willis, M., Kelleher, C., Cloutier, M., Husby, E., Foga, S., Nakamura,](#)
1218 [H., Platson, M., Wethington, M., Jr, Williamson, C., Bauer, G., Enos, J., Arnold, G., Kramer,](#)
1219 [W., Becker, P., Doshi, A., D’Souza, C., Cummens, P., Laurier, F., and Bojesen, M.: ArcticDEM,](#)
1220 <https://doi.org/10.7910/DVN/OHHUKH>, 2018.

1221 [Porter, S. C.: Equilibrium-line altitudes of late Quaternary glaciers in the Southern Alps, New](#)
1222 [Zealand, \[https://doi.org/10.1016/0033-5894\\(75\\)90047-2\]\(https://doi.org/10.1016/0033-5894\(75\)90047-2\), 1975.](#)

1223 [Porter, S. C.: Snowline depression in the tropics during the Last Glaciation, Quat. Sci. Rev., 20,](#)

Formatted: Justified, Space After: 12 pt

Formatted: Superscript

Formatted: Superscript

1253 [1067–1091, 2001.](#)

1254 [Rounce, D. R., Hock, R., Maussion, F., Hugonnet, R., Kochtitzky, W., Huss, M., Berthier, E.,](#)
1255 [Brinkerhoff, D., Compagno, L., Copland, L., Farinotti, D., Menounos, B., and McNabb, R. W.:](#)
1256 [Global glacier change in the 21st century: Every increase in temperature matters, *Science*, 379,](#)
1257 [78–83, 2023.](#)

1258 [Schaefer, J. M., Denton, G. H., Kaplan, M., Putnam, A., Finkel, R. C., Barrell, D. J. A.,](#)
1259 [Andersen, B. G., Schwartz, R., Mackintosh, A., Chinn, T., and Schlüchter, C.: High-frequency](#)
1260 [Holocene glacier fluctuations in New Zealand differ from the northern signature, *Science*, 324,](#)
1261 [622–625, 2009.](#)

1262 [Seguinot, J., Rogozhina, I., Stroeven, A. P., Margold, M., and Kleman, J.: Numerical simulations](#)
1263 [of the Cordilleran Ice Sheet through the last glacial cycle, *Cryosphere*, 10, 639–664, 2016.](#)

1264 [Shea, J. M., Marshall, S. J., and Livingston, J. M.: Glacier distributions and climate in the](#)
1265 [Canadian Rockies, *Arct. Antarct. Alp. Res.*, 36, 272–279, 2004.](#)

1266 [Sueyoshi, T., Ohgaito, R., Yamamoto, A., Chikamoto, M. O., Hajima, T., Okajima, H.,](#)
1267 [Yoshimori, M., Abe, M., O’ishi, R., Saito, F., Watanabe, S., Kawamiya, M., and Abe-Ouchi, A.:](#)
1268 [Set-up of the PMIP3 paleoclimate experiments conducted using an Earth system model,](#)
1269 [MIROC-ESM, *Geosci. Model Dev.*, 6, 819–836, 2013.](#)

1270 [Taylor, K. E., Stouffer, R. J., and Meehl, G. A.: An overview of CMIP5 and the experiment](#)
1271 [design, *Bull. Am. Meteorol. Soc.*, 93, 485–498, 2012.](#)

1272 [Tomkins, J. D., Lamoureux, S. F., and Sauchyn, D. J.: Reconstruction of climate and glacial](#)
1273 [history based on a comparison of varve and tree-ring records from Mirror Lake, Northwest](#)
1274 [Territories, Canada, *Quat. Sci. Rev.*, 27, 1426–1441, 2008.](#)

1275 [Tomkins, M. D., Dortch, J. M., Hughes, P. D., Huck, J. J., Pallàs, R., Rodés, Á., Allard, J. L.,](#)
1276 [Stimson, A. G., Bourlès, D., Rinterknecht, V., Jomelli, V., Rodríguez-Rodríguez, L., Copons, R.,](#)
1277 [Barr, I. D., Darvill, C. M., and Bishop, T.: Moraine crest or slope: An analysis of the effects of](#)
1278 [boulder position on cosmogenic exposure age, *Earth Planet. Sci. Lett.*, 570, 117092, 2021.](#)

1279 [Yukimoto, S., Kawai, H., Koshiro, T., Oshima, N., Yoshida, K., Urakawa, S., Tsujino, H.,](#)
1280 [Deushi, M., Tanaka, T., Hosaka, M., Yabu, S., Yoshimura, H., Shindo, E., Mizuta, R., Obata, A.,](#)
1281 [Adachi, Y., and Ishii, M.: The Meteorological Research Institute Earth System Model Version](#)
1282 [2.0, MRI-ESM2.0: Description and basic evaluation of the physical component, *Journal of the*](#)
1283 [Meteorological Society of Japan. Ser. II, 97, 931–965, 2019.](#)

1284 [Zemp, M., Nussbaumer, S. U., Gärtner-Roer, I., Bannwart, J., Paul, F., and Hoelzle, M.: Global](#)
1285 [Glacier Change Bulletin No. 4 \(2018-2019\), ISC\(WDS\)/IUGG\(IACS\)/UNEP/UNESCO/WMO,](#)
1286 [World Glacier Monitoring Service, 278 pp., <https://doi.org/10.5904/wgms-fog-2021-05>, 2021.](#)

